

1
2
3
4
5
6
7
8
9
10
11
12
13
14
15
16
17
18
19
20

Constraining the strength of the terrestrial CO₂ fertilization
effect in the Canadian Earth System Model version 4.2
(CanESM4.2)

Deleted: On c
Deleted: an
Deleted: s
Deleted: m

V. K. Arora and J. F. Scinocca.

Canadian Centre for Climate Modelling and Analysis, Environment and Climate Change Canada,
University of Victoria, Victoria, B.C., V8W 2Y2, Canada

25 **Abstract**

26

27 Earth system models (ESMs) explicitly simulate the interactions between the physical climate
28 system components and biogeochemical cycles. Physical and biogeochemical aspects of ESMs
29 are routinely compared against their observation-based counterparts to assess model performance
30 and to evaluate how this performance is affected by ongoing model development. Here, we assess
31 the performance of version 4.2 of the Canadian Earth system model against four, land carbon
32 cycle focused, observation-based determinants of the global carbon cycle and the historical global
33 carbon budget over the 1850-2005 period. Our objective is to constrain the strength of the
34 terrestrial CO₂ fertilization effect which is known to be the most uncertain of all carbon cycle
35 feedbacks. The observation-based determinants include 1) globally-averaged atmospheric CO₂
36 concentration, 2) cumulative atmosphere-land CO₂ flux, 3) atmosphere-land CO₂ flux for the
37 decades of 1960s, 1970s, 1980s, 1990s and 2000s and 4) the amplitude of the globally-averaged
38 annual CO₂ cycle and its increase over the 1980 to 2005 period. The optimal simulation that
39 satisfies constraints imposed by the first three determinants yields a net primary productivity
40 (NPP) increase from ~58 Pg C/yr in 1850 to about ~74 Pg C/yr in 2005; an increase of ~27% over
41 the 1850-2005 period. The simulated loss in the global soil carbon amount due to anthropogenic
42 land use change over the historical period is also broadly consistent with empirical estimates. Yet,
43 it remains possible that these determinants of the global carbon cycle are insufficient to
44 adequately constrain the historical carbon budget, and consequently the strength of terrestrial CO₂
45 fertilization effect as it is represented in the model, given the large uncertainty associated with
46 LUC emissions over the historical period.

47

48 **1. Introduction**

49

50 The evolution of the atmospheric CO₂ concentration in response to anthropogenic fossil fuel CO₂
51 emissions is determined by the rate at which a fraction of these emissions is taken up by the land
52 and ocean. Had the land and ocean not provided this “ecosystem service” since the start of the
53 industrial era, and not removed about 50% of CO₂ emissions from the atmosphere (Knorr, 2009),
54 the present concentration of CO₂ in the atmosphere would have been around 500 ppm, compared
55 to its current value of around 400 ppm. Over land, temperate and boreal forests as well as forests
56 in the tropical region are known to be sinks of atmospheric carbon (Ciais et al., 2013; Gourdji et
57 al., 2012; Schimel et al., 2015). The sink in the tropical forests is, however, compensated by
58 anthropogenic land use change emissions (Phillips and Lewis, 2014). Over ocean, the uptake of
59 anthropogenic carbon is observed to be larger in the high latitudes than in the tropical and
60 subtropical regions (Khatiwala et al., 2009). The manner in which the land and ocean will
61 continue to provide this ecosystem service in future is of both scientific and policy relevance.

62

63 Future projections of atmospheric CO₂ concentration, [CO₂], in response to continued
64 anthropogenic CO₂ emissions, or alternatively projections of CO₂ emissions compatible with a
65 given future [CO₂] pathway, are based primarily on comprehensive Earth system models (ESMs)
66 which include interactive land and ocean carbon cycle components (Jones et al., 2013). The land
67 and ocean carbon cycle components in ESMs respond both to increases in [CO₂] as well as the
68 associated changes in climate. These carbon components also respond to changes in climate
69 associated with other forcings including changes in concentration of non-CO₂ greenhouse gases
70 and aerosols, to nitrogen deposition and over land to anthropogenic land use change (LUC).

71

72 The response of land and ocean carbon cycle components to changes in [CO₂] and the associated
73 change in climate is most simply characterized in the framework of the 140-year long 1% per year
74 increasing CO₂ (1pctCO₂) experiment, in which [CO₂] increases at a rate of 1% per year from
75 pre-industrial value of about 285 ppm until concentration quadruples to about 1140 ppm. The
76 1pctCO₂ experiment has been recognized as a standard experiment by the coupled model
77 intercomparison project (CMIP) which serves to quantify the response of several climate and
78 Earth system metrics to increasing CO₂. These metrics include the transient climate response
79 (TCR) and the transient climate response to cumulative emissions (TCRE, Gillett et al., 2013).
80 Arora et al. (2013) analyzed results from fully-, biogeochemically- and radiatively-coupled
81 versions of the 1pctCO₂ experiment from eight ESMs that participated in the phase five of the
82 CMIP (CMIP5). They calculated the response of land and ocean carbon cycle components to
83 changes in [CO₂] and the associated change in climate expressed in terms of carbon-concentration
84 and carbon-climate feedbacks, respectively. Arora et al. (2013) found that of all the carbon cycle
85 feedbacks, the carbon-concentration feedback over land, which is primarily determined by the
86 strength of the terrestrial CO₂ fertilization effect, is the most uncertain across models. They found
87 that while the uncertainty in the carbon-concentration feedback over land (expressed in terms of
88 the standard deviation of the magnitude of the feedbacks) had somewhat reduced since the first
89 coupled carbon cycle climate model intercomparison project (C⁴MIP) (Friedlingstein et al., 2006)
90 its uncertainty remained the largest of all carbon cycle feedbacks. The comparison of the actual
91 magnitudes of the carbon cycle feedbacks over land is, however, not straightforward between the
92 Arora et al. (2013) and Friedlingstein et al. (2006) studies because they used different CO₂
93 scenarios.

94

95 The reason for this large uncertainty is that it is fairly difficult at present to constrain the strength
96 of the terrestrial CO₂ fertilization effect at the global scale. The net atmosphere-land CO₂ flux
97 since the start of the industrial era has not only been influenced by the changes in [CO₂] but also
98 the associated change in climate (due both to changes in [CO₂] and other climate forcings),
99 nitrogen deposition, and more importantly land use change - the contribution of which itself
100 remains highly uncertain. Since it is difficult to estimate the observed magnitude of net
101 atmosphere-land CO₂ flux since the start of the industrial era attributable only to increase in
102 [CO₂] it is consequently difficult to estimate the strength of the terrestrial CO₂ fertilization effect.

103

104 Measurements at Free-Air CO₂ Enrichment (FACE) sites in which vegetation is exposed to
105 elevated levels of [CO₂] help to assess some aspects of CO₂ fertilization and how nutrients
106 constraints regulate photosynthesis at elevated [CO₂] (Medlyn et al., 1999; McGuire et al., 1995).
107 However, FACE results cannot be easily extrapolated to the global scale and the response of
108 vegetation corresponds to a step increase in [CO₂] not the gradual increase which the real world
109 vegetation is experiencing.

110

111 As part of the ongoing evaluation of carbon cycle in ESMs, the model simulated aspects of the
112 global carbon cycle are routinely evaluated against their observation-based counterparts. These
113 evaluations also provide the opportunity to adjust physical processes that influence the strength of
114 the terrestrial CO₂ fertilization effect to provide the best comparison with observation-based
115 aspects of the global carbon cycle. Here, we present results from such an evaluation for a new
116 version of the Canadian Earth system model (CanESM4.2). An earlier version of the Canadian
117 Earth system model (CanESM2, Arora et al., 2011) participated in the CMIP5 (Taylor et al. 2012)

118 and its results also contributed to the fifth assessment report (AR5) of the Intergovernmental
119 Panel on Climate Change (IPCC). We evaluate the response of CanESM4.2, for three different
120 strengths of the terrestrial CO₂ fertilization effect, against four observation-based determinants of
121 the global carbon cycle and the historical global carbon budget over the 1850-2005 period, with a
122 focus on the land carbon cycle component. These determinants include 1) globally-averaged
123 atmospheric CO₂ concentration, 2) cumulative atmosphere-land CO₂ flux, 3) atmosphere-land
124 CO₂ flux for the decades of 1960s, 1970s, 1980s, 1990s and 2000s, and 4) the amplitude of the
125 globally-averaged annual CO₂ cycle and its increase over the 1980 to 2005 period.

126

127 The strength of the CO₂ fertilization effect influences all four of these determinants of the global
128 carbon cycle and the historical carbon budget. A stronger CO₂ fertilization effect, of course,
129 implies a larger carbon uptake by land and consequently a lower rate of increase of [CO₂] in
130 response to anthropogenic fossil fuel emissions. However, the strength of the CO₂ fertilization
131 effect also influences the amplitude of the annual [CO₂] cycle which is primarily controlled by the
132 northern hemisphere's biospheric activity. The amplitude of the annual [CO₂] cycle has been
133 observed to increase over the past five decades suggesting a gradual increase in photosynthesis in
134 association with a strengthening of the CO₂ fertilization effect (Keeling et al., 1996 ; Randerson et
135 al., 1997) and thus possibly can help to constrain the strength of the terrestrial CO₂ fertilization
136 effect in Earth system models.

137

138 **2. The coupled climate-carbon system and CanESM4.2**

139

140 **2.1 The coupled climate-carbon system**

141

142 The globally-averaged and vertically-integrated carbon budget for the combined atmosphere-
 143 land-ocean system may be written as:

$$\frac{dH_G}{dt} = \frac{dH_A}{dt} + \frac{dH_L}{dt} + \frac{dH_O}{dt} = E_F \quad (1)$$

144
 145 where the Global carbon pool $H_G = H_A + H_L + H_O$ is the sum of carbon in the Atmosphere, Land
 146 and Ocean components, respectively (Pg C), and E_F is the rate of anthropogenic CO₂ emissions
 147 (Pg C/yr) into the atmosphere. The equations for the atmosphere, land and ocean components are
 148 written as

$$\begin{aligned} \frac{dH_A}{dt} &= F_A + E_F \\ &= -F_L - F_O + E_F \\ &= -(F_l - E_L) - F_O + E_F \\ &= -F_l - F_O + E_F + E_L \end{aligned} \quad (2)$$

$$\frac{dH_L}{dt} = F_L = F_l - E_L$$

$$\frac{dH_O}{dt} = F_O$$

153 where $(F_L + F_O) = -F_A$ are the fluxes (Pg C/yr) between the atmosphere and the underlying land
 154 and ocean, taken to be positive into the components. The net atmosphere-land CO₂ flux
 155 $F_L = F_l - E_L$ is composed of LUC emission rate E_L (Pg C/yr) as well as the remaining global
 156 “natural” CO₂ flux F_l that is often referred to as the residual or missing land sink in the context of
 157 the historical carbon budget (Le Quéré et al., 2015). The emissions associated with LUC occur
 158 when natural vegetation, for example, is deforested and replaced by croplands resulting in net loss
 159 of carbon from land to the atmosphere (i.e. positive E_L). Conversely, when croplands are
 160

161 abandoned and gradually replaced by forests then carbon is gained from atmosphere into the land
 162 (i.e. negative E_L).

163
 164 Over land, the rate of change of carbon is reflected in the model's three land pools (vegetation, V ;
 165 soil, S ; and litter or detritus, D)

$$\begin{aligned}
 \frac{dH_L}{dt} &= F_L = F_l - E_L \\
 &= \frac{dH_V}{dt} + \frac{dH_S}{dt} + \frac{dH_D}{dt} \\
 &= (G - R_A) - R_H - E_L \\
 &= N - R_H - E_L
 \end{aligned}
 \tag{3}$$

167 where G is the gross primary productivity (Pg C/yr) which represents the rate of carbon uptake by
 168 vegetation through photosynthesis, and R_A and R_H are the autotrophic and heterotrophic
 169 respiratory fluxes (Pg C/yr) from living vegetation and dead litter and soil carbon pools,
 170 respectively. $N = G - R_A$ is the net primary productivity (NPP) which represents the carbon
 171 uptake by vegetation after autotrophic respiratory costs have been taken into account. The
 172 heterotrophic respiration $R_H = R_{H,D} + R_{H,S}$ is composed of respiration from the litter and soil
 173 carbon pools. The rate of change in carbon in model's litter (H_D) and soil (H_S) pools is written as

$$\begin{aligned}
 \frac{dH_D}{dt} &= D_L + D_S + D_R - C_{D \rightarrow S} - R_{H,D} \\
 \frac{dH_S}{dt} &= C_{D \rightarrow S} - R_{H,S}
 \end{aligned}
 \tag{4}$$

175 where $D_{i,i=L,S,R}$ is the litter fall from the model's Leaf, Stem and Root components into the
 176 model's litter pool. $C_{D \rightarrow S}$ is the transfer of humidified litter into the soil carbon pool calculated as
 177 a fraction of the litter respiration ($R_{H,D}$)

$$C_{D \rightarrow S} = \chi R_{H,D} \tag{5}$$

179 and χ is the humification factor.

180

181 Integrating (2) and (3) in time with $\int_{t_0}^t (dH/dt)dt = H(t) - H(t_0) = \Delta H(t)$ and $\int_{t_0}^t F dt = \tilde{F}(t)$ (Pg

182 C) gives

$$\begin{aligned}\Delta H_A &= -(\tilde{F}_O + \tilde{F}_I) + (\tilde{E}_F + \tilde{E}_L) \\ \Delta H_O &= \tilde{F}_O \\ \Delta H_L &= \tilde{F}_L = \tilde{F}_I - \tilde{E}_L; \\ &= \Delta H_V + \Delta H_S + \Delta H_D = \tilde{F}_I - \tilde{E}_L = \tilde{N} - \tilde{R}_H - \tilde{E}_L \\ \Delta H_I &= \tilde{F}_I \\ \Delta H &= \tilde{E}_F\end{aligned}\tag{6}$$

184 The cumulative change in the atmosphere, the ocean and the land carbon pools is written as

$$\begin{aligned}\Delta H_A + \Delta H_O + (\Delta H_L - \tilde{E}_L) &= \tilde{E}_F \\ \Delta H_A + \Delta H_O + \Delta H_L &= \tilde{E}_F + \tilde{E}_L = \tilde{E}\end{aligned}\tag{7}$$

186 where \tilde{E} (Pg C) is the cumulative sum of the anthropogenic emissions from fossil fuel
187 consumption and land use change. When emissions associated with LUC are zero, equation (7)

188 becomes

$$\Delta H_A + \Delta H_O + \Delta H_L = \tilde{E}_F = \tilde{E}\tag{8}$$

190 which indicates how cumulative emissions are parsed into changes in atmospheric carbon burden
191 and carbon uptake by the ocean and land components.

192

193 **2.2 Canadian Earth System Model version 4.2**

194

195 **2.2.1 Physical components**

196

197 At the Canadian Centre for Climate Modelling and Analysis (CCCma), the earth system model,
198 CanESM2, has undergone further development since its use for CMIP5. This version of the
199 model has been equivalently labelled CanESM4.0 in an effort to rationalize the ESM naming
200 convention to better reflect the fact that this model version employs the 4th generation atmosphere
201 component, CanAM4, (Von Salzen et al. 2013) and the 4th generation ocean component, CanOM4
202 (Arora et al., 2011). The version of the CCCma earth system model used for this study is
203 CanESM4.2 and so, represents two full cycles of model development on all of its components.
204 Similar to CanESM2, the physical ocean component of CanESM4.2 (CanOM4.2) has 40 levels
205 with approximately 10 m resolution in the upper ocean while the horizontal ocean resolution is
206 approximately 1.41° (longitude) \times 0.94° (latitude). The majority of development in CanESM4.2,
207 relative to CanESM2, has occurred on its atmospheric component CanAM4.2. CanAM4.2 is a
208 spectral model employing T63 triangular truncation with physical tendencies calculated on a 128
209 \times 64 ($\sim 2.81^\circ$) horizontal linear grid with 49 layers in the vertical whose thicknesses increase
210 monotonically with height to 1 hPa. Relative to CanAM4, CanAM4.2 includes a new version of
211 the Canadian Land Surface Scheme, CLASS3.6, which models the energy and water fluxes at the
212 atmosphere-land boundary by tracking energy and water through the soil, snow, and vegetation
213 canopy components (Verseghy, 2012). CLASS models the land surface energy and water balance
214 and calculates liquid and frozen soil moisture, and soil temperature for three soil layers (with
215 thicknesses 0.1, 0.25 and 3.75 m). The thickness of the third layer depends on the depth to
216 bedrock (and is in many places less than 3.75 m) based on the Zobler (1986) soil data set.
217 Changes to CLASS primarily include improvements to the simulation of snow at the land surface.
218 These incorporate new formulations for vegetation interception of snow (Bartlett et al., 2006), for

219 unloading of snow from vegetation (Hedstrom and Pomeroy, 1998), for the albedo of snow-
220 covered canopies (Bartlett and Verseghy, 2015), for limiting snow density as a function of depth
221 (Tabler et al., 1990; Brown et al., 2006), and for the thermal conductivity of snow (Sturm et al.,
222 1997). Water retention in snowpacks has also been incorporated. CanAM4.2 also includes an
223 aerosol microphysics scheme (von Salzen, 2006; Ma et al., 2008; Peng et al., 2012), a higher
224 vertical resolution in the upper troposphere, a reduced solar constant (1361W/m^2) and an
225 improved treatment of the solar continuum used in the radiative transfer. CanAM4.2 also
226 considers natural and anthropogenic aerosols and their emissions, transport, gas-phase and
227 aqueous-phase chemistry, and dry and wet deposition as summarized in Namazi et al. (2015)

228

229 **2.2.2 Land and ocean carbon cycle components**

230

231 The ocean and land carbon cycle components of CanESM4.2, are similar to CanESM2, and
232 represented by the Canadian Model of Ocean Carbon (CMOC) (Christian et al., 2010) and the
233 Canadian Terrestrial Ecosystem Model (CTEM) (Arora et al., 2009; Arora and Boer, 2010),
234 respectively.

235

236 LUC emissions in CTEM are modelled interactively on the basis of changes in land cover which
237 are determined by changes in crop area. The historical land cover used in the simulations
238 presented here is reconstructed using the linear approach of Arora and Boer (2010) and is the
239 same as used for CMIP5 simulations; as the fraction of crop area in a grid cell changes, the
240 fraction of non-crop plant functional types (PFTs) is adjusted linearly in proportion to their
241 existing coverage. The historical changes in crop area are based on the data set provided for

242 CMIP5 simulations as explained in Arora and Boer (2014). When the fraction of crop area in a
 243 grid cell increases then the fractional coverage of other PFTs is reduced which results in
 244 deforested biomass. The deforested biomass is allocated to three components that are i) burned
 245 instantaneously and contribute to ii) short (paper) and iii) long (wood products) term pools (Arora
 246 and Boer, 2010). The deforested biomass corresponding to paper and wood products is
 247 transferred to model's litter and soil carbon pools, respectively. When the fraction of crop area
 248 decreases, the fractional coverage of non-crop PFTs increases and their vegetation biomass is
 249 spread over a larger area reducing vegetation density. Carbon is sequestered until a new
 250 equilibrium is reached providing a carbon sink associated with regrowth as the abandoned areas
 251 revert back to natural vegetation.

252
 253 The LUC emissions term (E_L) in the equations (1) through (8) is not easily defined or calculated.
 254 Pongratz et al. (2014) discuss the multiple definitions and methods of calculating E_L . When E_L
 255 is calculated using models, it is most usually defined as the difference in F_L between simulations
 256 with and without LUC. This is also the basic definition used by Pongratz et al. (2014).
 257 Calculating E_L thus requires performing additional simulations without land use change in which
 258 land cover is held constant at its pre-industrial state. For a simulation without LUC equation (3)
 259 becomes

$$\frac{dH'_L}{dt} = F'_L = F'_i \quad (9)$$

261 and an estimate of E_L , and its cumulative values \tilde{E}_L , is obtained as

$$\begin{aligned} E_L &= F'_L - F_L \\ \tilde{E}_L &= \tilde{F}'_L - \tilde{F}_L \end{aligned} \quad (10)$$

263 Over the historical period, globally, F'_L is expected to be higher than F_L (both considered
264 positive downwards) due, at least, to two processes: 1) fraction of deforested biomass that is
265 burned and which contributes to short and long term product pools all release carbon to the
266 atmosphere, albeit at different time scales, 2) the area that is deforested and put under agricultural
267 use loses soil carbon and cannot sequester carbon in response to increase $[\text{CO}_2]$ since crops are
268 frequently harvested. As a result E_L is positive.

269
270 Relative to CanESM2, the version of CTEM employed in CanESM4.2, CTEM4.2, includes
271 changes to the humification factor (χ , see equations 4 and 5) which determines what fraction of
272 the humidified litter is transferred from litter (H_D) to the soil carbon pool (H_S). The value of χ
273 employed in CTEM4.2 has been changed for crop PFTs from 0.45 to 0.10, which decreases the
274 transfer of the humidified litter to the soil carbon pool. As a result, a decrease in global soil
275 carbon over the historical period is obtained as natural vegetation is replaced by croplands as is
276 seen in empirical measurements (Wei et al., 2014). This change in humification factor was
277 required despite the higher litter decomposition rates over croplands and is discussed in more
278 detail later in the results section. In addition, in CTEM4.2 the sensitivity of photosynthesis to soil
279 moisture is reduced for coupling to CLASS 3.6, especially for the broadleaf evergreen PFT
280 (which exists mainly in the tropics) to somewhat account for deep roots, for example, in the
281 Amazonian region (e.g. see da Rocha et al., 2004).

282
283 CTEM has always included a parameterization of photosynthesis down-regulation, which
284 represents acclimatization to elevated CO_2 in the form of a decline in maximum photosynthetic
285 rate. In the absence of explicit coupling of terrestrial carbon and nitrogen cycles this

286 parameterization yields a mechanism to reduce photosynthesis rates as [CO₂] increases. The
 287 photosynthesis down-regulation parameterization is described in detail in Arora et al. (2009) and
 288 is based on earlier simpler models which expressed net or gross primary productivity (NPP or
 289 GPP) as a logarithmic function of atmospheric CO₂ concentration (e.g. Cao et al., 2001;
 290 Alexandrov and Oikawa, 2002).

$$291 \quad G(t) = G_0 \left(1 + \gamma_p \ln \left(\frac{C(t)}{C_0} \right) \right) \quad (11)$$

292 where GPP at any given time, $G(t)$, is a function of its initial value G_0 , atmospheric CO₂
 293 concentration at time t , $C(t)$, and its initial value C_0 . The rate of increase of GPP is determined by
 294 the parameter γ_p (where p indicates the “potential” rate of increase of GPP with CO₂). The ratio
 295 of GPP in two different versions of a model in which GPP increases at different rates (γ_p and γ_d)
 296 is given by

$$297 \quad \xi(C) = \frac{1 + \gamma_d \ln(C/C_0)}{1 + \gamma_p \ln(C/C_0)}, \quad (12)$$

298
 299 where t is omitted for clarity. When $\gamma_d < \gamma_p$, the modelled potential gross photosynthesis rate
 300 (G_p), which is not constrained by nutrient limitation, can be multiplied by the scalar $\xi(C)$
 301 (equation 12) which yields the gross primary productivity (G) used in equation (3) that now
 302 increases in response to CO₂ increases at a rate determined by the value of γ_d (the subscript d
 303 indicates down-regulation).

$$304 \quad G = \xi(C) G_p . \quad (13)$$

305

306 A lower value of γ_d than γ_p yields a value of $\xi(C)$ that is less than one. As the concentration of
307 CO₂, expressed as C in equation (12), increases above its pre-industrial level C_0 (285 ppm), $\xi(C)$
308 progressively decreases resulting in a gross primary productivity G , which is less than the its
309 potential value G_p . Figure 1 shows the behaviour of $\xi(C)$ for $\gamma_p=0.95$ and three values of γ_d
310 (0.25, 0.4 and 0.55) corresponding to three different strengths of the terrestrial CO₂ fertilization
311 effect. A value of $\gamma_d = 0.25$ was used for CanESM2 to best simulate the globally-averaged
312 surface CO₂ concentration and cumulative 1850-2005 atmosphere-land CO₂ flux. CanESM2,
313 however, wasn't as rigourously evaluated as we have attempted here for CanESM4.2. Through
314 the parameter γ_d , the physical process of down-regulation has a direct influence on the strength
315 of the terrestrial CO₂ fertilization effect. In practice, different combinations of γ_d and γ_p are able
316 to yield very similar values of $\xi(C)$. Arora et al. (2009) calculated the value of γ_d based on
317 results from six studies, two of which were meta-analyses each based on 15 and 77 individual
318 studies, that grow plants in ambient and elevated CO₂ environment. Their results are equivalent to
319 $\gamma_d=0.46$ with a range from 0.22 to 0.63 for $\gamma_p=0.95$.

320
321 In Figure 1, while $\xi(C)$ decreases with an increase in atmospheric CO₂, indicating progressive
322 decline in photosynthesis due to nutrient limitation, the slope $\frac{d\xi}{dC}$ also decreases. Although a
323 second-order effect, this is a limitation of the current formulation of $\xi(C)$. A decreasing $\xi(C)$ as
324 CO₂ increases can eventually also lead to decrease in GPP although we have not seen this
325 behaviour up to CO₂ concentration of around 1000 ppm in simulations performed with CanESM2
326 (see Arora and Boer, 2014). While γ_d is used to model down-regulation of photosynthesis it may

327 also be used as a measure of the strength of the CO₂ fertilization effect. Lower values of γ_d
328 indicate higher down-regulation (see Figure 1) so higher values of γ_d imply higher strength of the
329 CO₂ fertilization effect. Finally, γ_d is specific to CTEM and as such the value of this parameter is
330 irrelevant to other models. More relevant for comparison with other models is the simulated rate
331 of increase of NPP over the historical period that a given value of γ_d yields.

332

333 **2.2.3 Treatment of CO₂ in the atmosphere**

334

335 The land and ocean components of the carbon cycle in CanESM4.2 are operable for two
336 experimental designs – 1) an emissions-driven mode, where the atmospheric CO₂ concentration is
337 a freely evolving 3D tracer in the model and 2) a concentrations-driven mode, where the
338 atmospheric CO₂ concentration is prescribed externally.

339

340 In the emissions-driven mode the anthropogenic CO₂ emissions (E_F) are specified and since the
341 interactive land and ocean carbon cycle components simulate the F_L and F_O terms, respectively,
342 the model is able to simulate the evolution of [CO₂] through the H_A term, which represents the
343 atmospheric carbon burden, in equation (2). This is referred to as the interactively simulated
344 [CO₂], or “free-CO₂” configuration. In this case, the model simulates the transport of CO₂ in the
345 atmosphere producing 3D structure, an annual cycle, and inter-annual variability.

346

347 In the concentrations-driven mode, the land and ocean CO₂ fluxes, F_L and F_O , remain
348 interactively determined so model results can be used to diagnose the E_F term (based on equation
349 2) that is compatible with a given [CO₂] pathway at the global scale. The concentrations-driven

350 mode can be executed in two CanESM4.2 configurations. In the first configuration, a single scalar
351 value of $[\text{CO}_2]$, which may be time evolving, is imposed at all geographical and vertical locations
352 in the model. This follows the CMIP5 prescription for concentrations-driven simulations and we
353 refer to it here as, “specified-CO2” concentrations-driven mode. In the second configuration, a
354 new approach for specifying CO_2 concentration has been implemented in CanESM4.2. In this
355 new approach, only the globally averaged concentration of CO_2 in the lowest model level is
356 constrained by the prescribed value. The geographical and vertical distribution of CO_2 in the
357 atmosphere and its annual cycle in this second configuration is otherwise free to evolve in the
358 same manner as in the emissions-driven, free-CO2, configuration. A relaxation timescale of one
359 day is employed in this new configuration and a fixed annual cycle, derived from the free-CO2
360 preindustrial control simulation, is imposed on the reference value of $[\text{CO}_2]$. The reference value
361 of $[\text{CO}_2]$ may additionally be specified as time evolving. We refer to this configuration as the
362 “relaxed-CO2” concentrations-driven mode. Aside from the relaxational constraint on the global-
363 mean surface value of $[\text{CO}_2]$, the atmospheric configuration for relaxed-CO2 is identical to that
364 for free-CO2 with zero emissions. As a consequence, the relaxed CO2 configuration allows the
365 same nonlinearity in the atmosphere-surface exchange of CO_2 as the free CO2 configuration
366 leading to nearly identical spatial distribution and seasonal cycle of atmosphere CO_2
367 concentrations. In this regard, the relaxed-CO2 configuration is physically more realistic than the
368 specified-CO2 configuration.

369
370 There are practical advantages to using the relaxed-CO2 configuration over the specified-CO2
371 configuration for concentrations-driven simulations. When spinning up land and ocean carbon
372 pools in a preindustrial control simulation, the model is executed in concentrations driven mode

373 to bring these pools into equilibrium with a prescribed CO₂ concentration. In earlier versions of
374 the CanESM, a specified-CO₂ configuration was used for this purpose. Beginning with version
375 4.1, the relaxed-CO₂ configuration is used for this purpose because it produces little or no drift
376 when used to initialize the free-CO₂ preindustrial control simulations. In fact, a relaxed-CO₂
377 preindustrial control simulation may be used as the control simulation for both emissions-driven
378 and (relaxed-CO₂) concentrations-driven experiments. This is not the case when the specified-
379 CO₂ is used as the configuration for concentration driven experiments.

380

381 **3. Experimental set up**

382

383 Three different kinds of experiments are performed for this study. The first is the standard 1% per
384 year increasing CO₂ experiment (1pctCO₂) performed for three different strengths of the
385 terrestrial CO₂ fertilization effect. The 1pctCO₂ is a concentration-driven experiment and we use
386 the “relaxed-CO₂” configuration to specify CO₂ in the atmosphere. The second experiment is the
387 CMIP5 1850-2005 historical experiment, referred to as esmhistorical following CMIP5
388 terminology, which is performed with specified anthropogenic CO₂ emissions (i.e. in emissions-
389 driven, or “free-CO₂”, mode), where [CO₂] is simulated interactively. Concentrations of non-CO₂
390 greenhouse gases and emissions of aerosols and their precursors are specified in the esmhistorical
391 experiment following the CMIP5 protocol. The third experiment is same as the esmhistorical
392 experiment but LUC is not permitted and the land cover remains at its 1850 value; referred to as
393 the esmhistorical_noluc experiment. Two ensemble members are performed for each of the three
394 versions of the esmhistorical and esmhistorical_noluc experiments corresponding to three
395 different strengths of the terrestrial CO₂ fertilization effect. The rationale for performing historical

396 simulations without LUC is to be able to quantify LUC emissions E_L using equation (10). Table
397 1 summarizes all the simulations performed.

398
399 The 1pctCO2 simulations with “relaxed” CO₂ for three different strengths of the terrestrial CO₂
400 fertilization effect are initialized from a corresponding pre-industrial control simulation with CO₂
401 specified at ~285 ppm and all other forcings at their 1850 values. The esmhistorical and
402 esmhistorical_noluc simulations are initialized from a pre-industrial control simulation with
403 “free” CO₂ and zero anthropogenic CO₂ emissions.

404

405 **4. Results**

406

407 **4.1. 1% per year increasing CO₂ experiments**

408

409 Figure 2 shows the carbon budget components of equation (8); ΔH_A , ΔH_O and ΔH_L i.e. the
410 change in atmospheric carbon burden and cumulative atmosphere-ocean and atmosphere-land
411 CO₂ flux which together make up the cumulative diagnosed emissions (\tilde{E}) based on results from
412 the fully-coupled 1pctCO2 experiment. Results are shown from eight CMIP5 models that
413 participated in the Arora et al. (2013) study, including CanESM2 which used $\gamma_d=0.25$, together
414 with those from CanESM4.2 for three different strengths of the terrestrial CO₂ fertilization effect.
415 The cumulative atmosphere-land CO₂ flux across models varies much more than the cumulative
416 atmosphere-ocean CO₂ flux across the CMIP5 models as already noted in Arora et al. (2013). The
417 results for CanESM4.2 indicate that the influence of γ_d (equation 12) on the strength of the
418 model’s terrestrial CO₂ fertilization effect allows CanESM4.2’s cumulative diagnosed emissions
419 to essentially span the range of the other CMIP5 models. For the three different strengths of the

420 terrestrial CO₂ fertilization effect, $\gamma_d = 0.25, 0.4$ and 0.55 , the γ_d values of 0.4 and 0.55 yield
421 cumulative atmosphere-land CO₂ flux that is higher than all the CMIP5 models. The basis for
422 choosing these values of γ_d within the range 0.4 ± 0.15 is that they span the observation-based
423 estimates of various quantities reasonably well as shown later.

424
425 The cumulative atmosphere-land CO₂ flux ΔH_L for CanESM4.2 for the simulation with $\gamma_d=0.25$
426 is higher than that for CanESM2 which also uses $\gamma_d=0.25$, because of the changes made to soil
427 moisture sensitivity of photosynthesis and because ΔH_L also depends on the model climate. In
428 particular, the CanESM2 bias of low precipitation over the Amazonian region has been reduced
429 in CanESM4.2, as shown in Figure 3. The increased precipitation over the Amazonian region
430 causes increased carbon uptake with increasing [CO₂]. The improved precipitation bias of
431 CanESM4.2 in this region is in part caused by the decreased sensitivity of photosynthesis to soil
432 moisture in CTEM4.2, especially for broadleaf evergreen PFT, which helps to increase
433 evapotranspiration and in turn increase precipitation over the region.

434

435 **4.2. Historical simulations with LUC**

436

437 The results presented in this section evaluate the model against four observation-based
438 determinants of the global carbon cycle and the historical global carbon budget over the 1850-
439 2005 period mentioned earlier. Simulated atmosphere-ocean CO₂ fluxes are also compared with
440 observation-based estimates although, of course, they are not directly affected by the strength of
441 the terrestrial CO₂ fertilization effect.

442

443 **4.2.1. Components of land carbon budget**

444

445 In Figure 4, time series of instantaneous (F_L panel a) and cumulative (\tilde{F}_L panel b) atmosphere-
446 land CO₂ flux over the period 1850-2005 are displayed for CanESM2 (which contributed results
447 to CMIP5) and CanESM4.2 for the three different strengths of the terrestrial CO₂ fertilization
448 effect. The observation-based estimates of $F_L = (F_l - E_L)$ in Figure 4a for the decades of 1960,
449 1970, 1980, 1990 and 2000 are reproduced from Le Quéré et al. (2015) who derive the
450 $F_L = (F_l - E_L)$ term as residual of the carbon budget equation $dH_A/dt = -(F_l - E_L) - F_O + E_F$
451 using observation-based estimates of change in atmospheric carbon budget (dH_A/dt),
452 atmosphere-ocean CO₂ flux (F_O) and fossil fuel emissions (E_F). The observation-based estimate
453 of -11 ± 47 Pg C in Figure 4b for \tilde{F}_L over the period 1850-2005 is from Arora et al. (2011) (their
454 Table 1).

455

456 The primary difference between CanESM2 and CanESM4.2 simulations in Figure 4 is that \tilde{F}_L for
457 CanESM2 generally stays positive throughout the historical period, whereas for CanESM4.2 it
458 first becomes negative (indicating that land is losing carbon) and then becomes positive
459 (indicating that land is gaining carbon) towards the end of the 20th century, depending on the
460 strength of the CO₂ fertilization effect. The behaviour of \tilde{F}_L for CanESM4.2 is considered to be
461 more realistic. As the land responds to anthropogenic land use change, associated with an increase
462 in crop area early in the historical period, it causes a decrease in vegetation and soil carbon (see
463 Figure 5). Later in the 20th Century, the CO₂ fertilization effect causes the land to become a sink
464 for carbon resulting in both vegetation and soil carbon increases. This behavior is consistent with
465 the mean model response of the 15 CMIP5 models analyzed by Hoffman et al. (2013) (their

466 Figure 2b). In contrast, CanESM2 shows a gradual increase in the global soil carbon amount
467 (Figure 5a) over the historical period. In Figure 5, it can be seen that the effect of CO₂ fertilization
468 in the second half of the 20th century is delayed for soil carbon compared to that for vegetation.
469 This is primarily because of the lag introduced by the turnover time of vegetation (i.e., increased
470 NPP inputs have to go through vegetation pool first) and the longer turnover time scale of the soil
471 carbon pool. The more reasonable response of soil carbon to anthropogenic land use change, in
472 Figure 5a for CanESM4.2, is achieved by changing the humification factor from 0.45 (in
473 CanESM2) to 0.10 (in CanESM4.2) in equation (5) which yields a reduction in global soil carbon
474 amount in response to land use change up until the time that the effect of CO₂ fertilization starts
475 to take effect. In Figure 4a, CanESM4.2 is also able to simulate continuously increasing F_L during
476 the period 1960 to 2005, depending on the strength of the CO₂ fertilization effect, while
477 CanESM2 simulates near constant or decreasing F_L from about 1990 onwards, as is also seen in
478 Figure 4b for \tilde{F}_L . This behaviour of F_L is not consistent with observation-based estimates from
479 Le Quéré et al. (2015) which show continued strengthening of the land carbon sink since 1960s.

480
481 In Figure 4a, amongst the three versions of the CanESM4.2, the simulation with $\gamma_d = 0.4$ (blue
482 line) yields the best comparison with observation-based estimates of F_L from Le Quéré et al.
483 (2015), while the simulations with $\gamma_d = 0.25$ (green line) and $\gamma_d = 0.55$ (red line) yield F_L values
484 that are lower and higher, respectively, than observation-based estimates. In Figure 4b, the
485 cumulative atmosphere-land CO₂ flux \tilde{F}_L over the 1850-2005 period from the simulations with
486 $\gamma_d = 0.25$ and 0.4 (green and blue lines, respectively) lies within the uncertainty of observation-

487 based estimates, while the simulation with $\gamma_d = 0.55$ (red line) yields \tilde{F}_L value that is high
488 relative to observation-based estimate.

489
490 Figure 6 shows the change in and absolute values of NPP from CanESM2 and the simulations
491 made with CanESM4.2 for three different strengths of the CO₂ fertilization effect. Consistent with
492 1pctCO2 simulations, the rate of increase of NPP in CanESM4.2 with $\gamma_d = 0.25$ is higher than
493 that in CanESM2 which also uses $\gamma_d = 0.25$. This is because the underlying model climate is
494 different in CanESM2 and CanESM4.2, as mentioned earlier, and the fact that photosynthesis
495 sensitivity to soil moisture has also been reduced. The rates of increase of NPP for $\gamma_d = 0.40$ and
496 0.50 are, of course, even higher. The CanESM4.2 simulation with $\gamma_d = 0.40$, which yields the
497 best comparison with observation-based estimates of F_L for the decade of 1960 through 2000
498 (Figure 4a) as well as \tilde{F}_L for the period 1850-2005 (Figure 4b), yields an increase in NPP of ~16
499 Pg C/yr over the 1850-2005 period. A caveat here is that part of this increase is also caused by
500 increase in the crop area over the historical period that is realized in the model regardless of the
501 strength of the CO₂ fertilization effect. In CTEM, the maximum photosynthetic capacity of crops
502 is higher than for other PFTs to account for the fact that agricultural areas are generally fertilized.
503 As a result, increase in crop area also increases global NPP. The increasing crop productivity has
504 been suggested to contribute to the increase in amplitude of the annual [CO₂] cycle since 1960s
505 (Zeng et al., 2014). However, in the absence of an explicit representation of terrestrial N cycle
506 (and thus fertilization of cropped areas) or a representation of increase in crop yield per unit area
507 due to genetic modifications, the only processes in CTEM that contribute to changes in crop yield
508 are the change in crop area itself and the increase in crop NPP due to the CO₂ fertilization effect.

509

510 **4.2.2. Globally-averaged [CO₂]**

511

512 Figure 7 shows the simulated globally-averaged surface [CO₂] from the emissions-driven
513 esmhistorical simulation of CanESM2 and that of CanESM4.2 for three different strengths of the
514 CO₂ fertilization effect. The observation-based time series of [CO₂] is illustrated by the heavy
515 black line. The CanESM2 ($\gamma_d=0.25$) simulation yields a reasonable comparison with observation-
516 based [CO₂]. Amongst the versions of CanESM4.2 with different strengths of the CO₂
517 fertilization effect, the version with $\gamma_d=0.40$ yield the best comparison. The CanESM4.2 version
518 with $\gamma_d=0.25$ (weaker strength of the CO₂ fertilization effect) and 0.55 (stronger CO₂ fertilization
519 effect) yield CO₂ concentrations that are respectively higher and lower than the observational
520 estimate from roughly mid-20th Century onward. The reason CanESM4.2 ($\gamma_d=0.40$) requires a
521 stronger CO₂ fertilization effect than CanESM2 ($\gamma_d=0.25$) for simulating the observation-based
522 increase in atmospheric CO₂ burden over the historical period is the enhanced impact of LUC in
523 CanESM4.2 due to its increased humification factor and the associated response of the global soil
524 carbon pool, as discussed in the previous section. The differences in simulated [CO₂] in Figure 7
525 from CanESM4.2 are due only to differences in the strength of the CO₂ fertilization effect.
526 Although, of course, since in these simulations [CO₂] is simulated interactively, the simulated
527 atmosphere-land flux F_L and [CO₂] both respond to and affect each other.

528

529 Both CanESM2 and CanESM4.2 underpredict [CO₂] relative to observational estimates over the
530 period 1850-1930, and are also unable to reproduce the near zero rate of increase of [CO₂] around
531 1940. Possible reasons for these discrepancies include 1) the possibility that carbon cycle before

532 1850 was not in true equilibrium and this aspect cannot be captured since the model is spun up to
533 equilibrium for 1850 conditions, 2) the uncertainties associated with anthropogenic emissions for
534 the late 19th and early 20th century that are used to drive the model, and 3) the uncertainties
535 associated with pre Mauna-Loa [CO₂] observations.

536

537 **4.2.3. Atmosphere-ocean CO₂ flux**

538

539 Figures 8a and b, respectively, show time series of instantaneous (F_O) and cumulative (\tilde{F}_O)
540 atmosphere-ocean CO₂ fluxes over the period 1850-2005 for the set of emissions-driven
541 simulations presented in Fig. 7. The strength of the terrestrial CO₂ fertilization effect has little or
542 no impact on the ocean biogeochemical processes. The differences in values of F_O and \tilde{F}_O for
543 the three versions CanESM4.2 are, therefore, primarily due to the differences in [CO₂]. The
544 observation-based estimates of F_O in Figure 8a for the decades of 1960, 1970, 1980, 1990 and
545 2000 are from Le Quéré et al. (2015). The observation-based estimate of \tilde{F}_O of 141 ± 27 Pg C in
546 Figure 8b for the period 1850-2005 is from Arora et al. (2011) (their Table 1).

547

548 Both CanESM2 and the CanESM4.2 simulation for $\gamma_d=0.40$ (which provides the best comparison
549 with observation-based estimate for [CO₂]; blue line in Figure 7) yield lower \tilde{F}_O compared to
550 observation-based values. The F_O value from CanESM2 and the CanESM4.2 simulation for
551 $\gamma_d=0.40$ are lower than the mean estimates from Le Quéré et al. (2015) for the decades of 1960s
552 through 2000s, although still within their uncertainty range. The family of ESMs from CCCma,
553 all of which have the same physical ocean model, including CanESM1 (Arora et al., 2009),

554 CanESM2 (Arora et al., 2011) and now CanESM4.2, yield lower than observed ocean carbon
555 uptake over the historical period. Recent analyses of these model versions suggest that the
556 primary reason for their low carbon uptake is a negative bias in near surface wind speeds over the
557 Southern Ocean and an iron limitation in the same region which is too strong (personal
558 communication, Dr. Neil Swart, Canadian Centre for Climate Modelling and Analysis). The
559 CanESM4.2 simulation with $\gamma_d=0.25$ (green line in Figure 8) yields a better comparison with
560 observation-based estimates of F_o and \tilde{F}_o but that is because of the higher simulated $[\text{CO}_2]$ in
561 that simulation associated with lower carbon uptake by land.

562

563 **4.2.4. Amplitude of the annual CO₂ cycle**

564

565 The annual CO₂ cycle is influenced strongly by the terrestrial biospheric activity of the northern
566 hemisphere (Keeling et al., 1996; Randerson et al., 1997). Higher than normal biospheric uptake
567 of carbon during a northern hemisphere's growing season, for example, will yield lower than
568 normal $[\text{CO}_2]$ by the end of the growing season, around September when $[\text{CO}_2]$ is at its lowest
569 level (see Figure 9a). Similarly, during the northern hemisphere's dormant season, increased
570 respiration from live vegetation and decomposition of dead carbon, including leaf litter, that may
571 be associated with increased carbon uptake during the last growing season, will yield higher than
572 normal $[\text{CO}_2]$ during April when $[\text{CO}_2]$ is at its highest level. Both processes increase the
573 amplitude of the annual $[\text{CO}_2]$ cycle. Given this strong control, the rate of change of the
574 amplitude of the annual $[\text{CO}_2]$ cycle can potentially help to constrain the strength of the terrestrial
575 CO₂ fertilization effect.

576

577 Figure 9a compares the annual cycle of the trend-adjusted globally-averaged near-surface
578 monthly [CO₂] anomalies from CanESM2 and the versions of CanESM4.2 for three different
579 strengths of the CO₂ fertilization effect with observation-based estimates for the 1991-2000
580 period. Figure 9b shows the time series of the amplitude of the annual cycle of the trend adjusted
581 globally-averaged near-surface monthly [CO₂] anomalies (referred to as Φ_{CO_2}) from CanESM2
582 and CanEM4.2, as well as observation-based estimates going back to 1980s. While CO₂
583 measurements at Mauna Loa started in 1959, observation-based globally-averaged near-surface
584 [CO₂] values are only available since 1980s
585 (ftp://aftp.cmdl.noaa.gov/products/trends/co2/co2_mm_gl.txt). In Figure 9b, consistent with the
586 strengthening of the CO₂ fertilization effect, associated with the increase in [CO₂], the
587 observation-based estimate of Φ_{CO_2} shows an increase from 1980s to the present. Both CanESM2
588 and versions of CanESM4.2 also show an increase in the amplitude of Φ_{CO_2} over the period
589 1850-2005. However, the absolute values of Φ_{CO_2} are lower in CanESM2 than in CanESM4.2
590 (Figure 9b). Of course, in the absence of an observation-based estimate of pre-industrial value of
591 Φ_{CO_2} it is difficult to say which value is more correct. However, when considering the present
592 day values of Φ_{CO_2} the three versions of CanESM4.2 yield better comparison with observation-
593 based estimate as also shown in Figure 9a. The increase in the value of Φ_{CO_2} from CanESM2 to
594 CanESM4.2, which now yields better comparison with observation-based value of Φ_{CO_2} , is most
595 likely caused by the change in the land surface scheme from CLASS 2.7 (that is implemented in
596 CanESM2) to CLASS 3.6 (implemented in CanESM4.2), since the atmospheric component of the
597 model hasn't changed substantially. It is, however, difficult to attribute the cause of this
598 improvement in the present day value of Φ_{CO_2} in CanESM4.2 to a particular aspect of the new

599 version of the land surface scheme. The annual [CO₂] cycle is driven primarily by the response of
600 the terrestrial biosphere to the annual cycle of temperature and the associated greening of the
601 biosphere every summer in the northern hemisphere. However, the simulated amplitude of the
602 annual cycle of near-surface temperature hasn't changed substantially from CanESM2 to
603 CanESM4.2 (not shown).

604
605 In Figure 9b, the simulated values of Φ_{CO_2} for the CanESM4.2 simulations with $\gamma_d=0.25, 0.40$
606 and 0.55 are 4.41, 4.69 and 4.85 ppm, respectively, averaged over the period 1991-2000,
607 compared to observation-based value of Φ_{CO_2} of 4.36 ppm. Here, CanESM4.2 simulation with
608 $\gamma_d=0.25$ yields the best comparison with observation-based value of Φ_{CO_2} . An increase in the
609 strength of the CO₂ fertilization effect increases the amplitude of the annual [CO₂] cycle so a
610 larger value of γ_d yields a larger value of Φ_{CO_2} . The increase in the amplitude of the annual
611 [CO₂] cycle comes both from lower [CO₂] at the end of the growing season in September as well
612 as higher [CO₂] at the start of the northern hemisphere's growing season in April (see Figure 9a),
613 as mentioned earlier in this section.

614
615 More important than the absolute value of Φ_{CO_2} is its rate of increase over time which is a
616 measure of the strength of the terrestrial CO₂ fertilization effect. Figure 9b also shows the trend in
617 Φ_{CO_2} over the 1980-2005 overlapping period for which for both the model and observation-based
618 estimates of Φ_{CO_2} are available. The magnitude of trend for observation-based estimate of Φ_{CO_2}
619 is 0.142 ± 0.08 ppm/10-years (mean \pm standard deviation, $\bar{x} \pm \sigma_x$), implying that over the 26 year
620 1980-2005 period the amplitude of annual [CO₂] cycle has increased by 0.37 ± 0.21 ppm. The

621 calculated mean and standard deviation of the observation-based trend, however, does not take
622 into account the uncertainty associated with the observation-based estimates of $[\text{CO}_2]$,
623 consideration of which will increase the calculated standard deviation even more. The magnitudes
624 of trend in Φ_{CO_2} simulated by CanESM2 ($\gamma_d=0.25$) and CanESM4.2 (for $\gamma_d=0.25$) are
625 0.103 ± 0.05 and 0.153 ± 0.031 , respectively, and statistically not different from the trend in the
626 observation-based value of Φ_{CO_2} implying an increase of 0.27 ± 0.13 and 0.40 ± 0.08 ppm,
627 respectively, in Φ_{CO_2} over the 1980-2005 period. The statistical difference is calculated on the
628 basis of $\bar{x} \pm 1.385 \sigma_x$ range which corresponds to 83.4% confidence intervals; the estimates from
629 two sources are statistically not different at the 95% confidence level if this range overlaps (Knol
630 et al., 2011). The magnitudes of the trend in Φ_{CO_2} over the 1980-2005 period for CanESM4.2
631 simulations with $\gamma_d = 0.4$ and 0.55 (0.328 ± 0.038 and 0.314 ± 0.034 ppm/10-years, respectively)
632 are, however, more than twice, and statistically different from the observation-based estimate
633 (0.142 ± 0.08 ppm/10-years).

634
635 Overall, the CanESM4.2 simulation with $\gamma_d=0.25$ yields the amplitude of the globally-average
636 annual CO_2 cycle and its rate of increase over the 1980-2005 period that compares best with
637 observation-based estimates.

638

639 **4.3. Historical simulations without LUC**

640

641 Figure 10 and 11 show results from CanESM4.2 emissions-driven simulations for three different
642 strengths of the CO_2 fertilization effect that do not implement anthropogenic LUC over the
643 historical period and compare them to their corresponding simulations with LUC.

644
645 Figure 10a compares the simulated $[\text{CO}_2]$; as expected in the absence of anthropogenic LUC the
646 simulated $[\text{CO}_2]$ is lower since LUC emissions do not contribute to increase in $[\text{CO}_2]$. The
647 difference in $[\text{CO}_2]$ at the end of the simulation, in year 2005, between simulations with and
648 without LUC is 29.0, 23.6 and 19.0 ppm for $\gamma_d=0.25$, 0.40 and 0.55. The simulations with the
649 lowest strength of the CO_2 fertilization effect ($\gamma_d=0.25$) yield the largest difference because these
650 simulations also have the largest $[\text{CO}_2]$ amongst their set of simulations with and without LUC.
651 The CO_2 fertilization of the terrestrial biosphere implies that the effect of deforestation will be
652 higher, because of reduced carbon uptake by deforested vegetation, if background $[\text{CO}_2]$ is
653 higher.

654
655 Figure 10b compares the simulated NPP from CanESM4.2 simulations with and without LUC.
656 The increase in simulated NPP, regardless of the strength of the CO_2 fertilization effect, is lower
657 over the historical period in simulations without LUC for two apparent reasons. First, the rate of
658 increase of $[\text{CO}_2]$ is itself lower and second, in the absence of LUC, there is no contribution from
659 increasing crop area to NPP. Overall, the increase in NPP over the 1850-2005 period in
660 simulations with LUC is a little more than twice that in simulations without LUC. Figure 10c and
661 10d compare the changes in global vegetation biomass and soil carbon mass, over the historical
662 period, from simulations with and without LUC. As expected, in the absence of LUC, global
663 vegetation biomass and soil carbon mass more or less show a continuous increase, associated with
664 the increase in NPP which itself is due to the increase in $[\text{CO}_2]$. Consequently, in Figure 11a, the
665 cumulative atmosphere-land CO_2 flux \tilde{F}_L in simulations without LUC also shows a more or less
666 continuous increase over the historical period.

667
668 Finally, Figure 11b shows the diagnosed cumulative LUC emissions \tilde{E}_L calculated as the
669 difference between cumulative \tilde{F}_L , following equation 10, from simulations with and without
670 LUC. The diagnosed \tilde{E}_L in this manner are equal to 95, 81 and 67 Pg C, over the 1850-2005
671 period, for $\gamma_d=0.25$, 0.40 and 0.55. The calculated diagnosed \tilde{E}_L are highest for $\gamma_d=0.25$
672 associated with the highest background simulated $[\text{CO}_2]$ in these simulations, as mentioned
673 earlier. For comparison, LUC emissions estimated by Houghton (2008) for the period 1850-2005,
674 based on a book-keeping approach, are 156 Pg C but these estimates are generally believed to be
675 $\pm 50\%$ uncertain (see Figure 1 of Ramankutty et al. (2007)). LUC emissions, when calculated by
676 differencing F_L from simulations with and without LUC, also depend on the type of simulations
677 performed - in particular, if simulations are driven with specified CO_2 concentrations or specified
678 CO_2 emissions. Had our simulations been concentration-driven, in contrast to being emissions
679 driven, then both with and without LUC simulations would have experienced the same specified
680 observed CO_2 concentration over the historical period and the simulated LUC emissions would
681 have been higher. Arora and Boer (2010) found that diagnosed LUC emissions in the first version
682 of the Canadian Earth System Model (CanESM1) increased from 71 Pg C (for emissions-driven
683 simulations) to 124 Pg C (for concentration-driven simulations). Concentration-driven
684 simulations, however, cannot be evaluated against observation-based amplitude of the annual CO_2
685 cycle and its increase over the historical period. These simulations either ignore the annual cycle
686 of CO_2 (our specified- CO_2 case) or use a specified amplitude of the CO_2 annual cycle (our
687 relaxed- CO_2 case).

688

689 **5.0. Discussion and conclusions**

690

691 This study evaluates the ability of four observation-based determinants of the global carbon cycle
692 and the historical carbon budget to constrain the parameterization of photosynthesis down-
693 regulation, which directly determines the strength of the CO₂ fertilization effect, over the
694 historical period 1850-2005. The key parameter that controls the strength of the CO₂ fertilization
695 effect in CTEM, γ_d , was varied in the latest version of CCCma's earth system model CanESM4.2.
696 Comparing simulated and observation-based estimates of 1) globally-averaged atmospheric CO₂
697 concentration, 2) cumulative atmosphere-land CO₂ flux, and 3) atmosphere-land CO₂ flux for the
698 decades of 1960s, 1970s, 1980s, 1990s and 2000s, it is found that the CanESM4.2 version with
699 $\gamma_d=0.40$ yields the best comparison.

700

701 The evaluation of CTEM within the framework of CanESM4.2 presented here is based on an
702 emergent model property at the global scale and may be considered as a top-down approach of
703 model evaluation. In contrast, the bottom-up approaches of model evaluation typically evaluate
704 model results and processes against observations of primary atmosphere-land carbon and/or
705 nitrogen fluxes and sizes of the vegetation, litter and soil carbon/nitrogen pools (e.g. Zaehle et
706 al., 2014). Indeed, CTEM has been evaluated at point (e.g. Arora and Boer, 2005; Melton et al.,
707 2015), regional (e.g. Peng et al., 2014; Garnaud et al., 2014) and global (e.g. Arora and Boer,
708 2010; Melton and Arora, 2014) scales in a number of studies when driven with observation-based
709 reanalysis data. Both top-down and bottom-up approaches of model evaluation are complimentary
710 to each other and allow to evaluate different aspects of the model at different spatial and temporal
711 scales.

712

713 For the top-down approach used here, CanESM4.2 simulates globally-averaged near-surface
714 [CO₂] of 400, **381** and 368 ppm for $\gamma_d=0.25$, **0.40** and 0.55, respectively, compared to the
715 observation-based estimate of **379** ppm for year 2005. The cumulative atmosphere-land CO₂ flux
716 of 18 Pg C for the period 1850-2005 for $\gamma_d=0.40$ lies within the range of the observation-based
717 estimate of -11 ± 47 Pg C in Figure 4b, and so do the average atmosphere-land CO₂ flux for the
718 decades of 1960s through to 2000s in Figure 4a when compared to observation-based estimates
719 from Le Quéré et al. (2015). $\gamma_d=0.25$ and 0.55 yield average atmosphere-land CO₂ flux for the
720 decades of 1960s through to 2000s that are lower and higher, respectively, than the observation-
721 based estimates from Le Quéré et al. (2015). The only determinant against which $\gamma_d=0.40$ does
722 not yield the best comparison with observation-based estimates is the amplitude of the globally-
723 averaged annual CO₂ cycle and its increase over the 1980 to 2005 period. For this determinant,
724 $\gamma_d=0.25$ seems to yield the best comparison (Figure 9). The value of $\gamma_d=0.40$ that yields best
725 overall comparison with observation-based determinants of the global carbon cycle and the
726 historical carbon budget is also broadly consistent with Arora et al. (2009) who derived a value of
727 $\gamma_d=0.46$ based on results from FACE studies (as mentioned in Section 2.2.2).

728
729 The caveat with the analyses presented here, or for any model for that matter, is that the strength
730 of the terrestrial CO₂ fertilization effect is dependent on the processes included in the model and
731 the parameter values associated with them. The primary example of this is the adjustment to the
732 humification factor in CTEM4.2, which leads to reduction in the global soil carbon amount as
733 anthropogenic LUC becomes significant towards the mid-20th Century. This response of soil
734 carbon was not present in the model's configuration of CTEM and historical simulations made
735 with CanESM2. The representation of soil carbon loss, in response to anthropogenic LUC in

736 CanESM4.2, implies that a stronger CO₂ fertilization effect (or weaker photosynthesis down-
737 regulation) should be required to reproduce realistic atmosphere-land CO₂ flux over the historical
738 period and this was found to be the case in Figure 4a. Despite this dependence on processes
739 included in the model, the response of the land carbon cycle, over the historical period, to the two
740 primary forcings of increased [CO₂] and anthropogenic land use change must be sufficiently
741 realistic in the model to satisfy all the four determinants of the global carbon cycle and the
742 historical global carbon budget.

743
744 The simulated loss in soil carbon in response to anthropogenic LUC over the historical period
745 may also be assessed against observation-based estimates from Wei et al. (2014). Using data from
746 453 sites that were converted from forest to agricultural land, Wei et al. (2014) find that the soil
747 organic carbon stocks decreased by an average of $43.1 \pm 1.1\%$ for all sites. Based on the HYDE
748 v3.1 data set from which the changes in crop area are derived (Hurtt et al., 2011), LUC as
749 implemented in CanESM4.2 yields an increase in crop area from about 5 million km² in 1850 to
750 about 15 million km² in 2005. Assuming an initial soil carbon amount of 10 Kg C/m² (see Figure
751 2c of Melton and Arora (2014)) and an average 40% decrease in soil carbon amount, based on
752 Wei et al. (2014), implies that the increase in crop area of about 10 million km² over the historical
753 period has likely yielded a global soil organic carbon loss of 40 Pg C. The loss in soil carbon in
754 Figure 5a is simulated to 18 Pg C for CanESM4.2 simulation with $\gamma_d = 0.40$, the simulation that
755 yield best comparison with observation-based determinants of the global carbon cycle and the
756 historical carbon budget. This loss of 18 Pg C is expected to be less than the 40 Pg C because the
757 model estimates also include an increase associated with the increase in NPP due to the CO₂
758 fertilization effect from non-crop areas. The effect of LUC on global soil carbon loss may also by

759 estimated by differencing global soil carbon amounts from simulations with and without LUC
760 from Figure 10d at the end of the simulation in year 2005. For CanESM4.2 simulation with $\gamma_d =$
761 0.40, this amounts to around 50 Pg C. Both these estimates of soil carbon loss are broadly
762 consistent with the back-of-the-envelope calculation of 40 Pg C soil carbon loss, based on Wei et
763 al. (2014) estimates, indicating that the soil carbon loss simulated in response to anthropogenic
764 LUC over the historical period is not grossly over or underestimated.

765
766 The CanESM4.2 simulation with $\gamma_d = 0.40$, however, fails to satisfy the rate of increase of the
767 amplitude of the globally-averaged annual CO₂ cycle over the 1980-2005 period implying that
768 there are still limitations in the model structure and/or parameter values. Of course, the fact that
769 the amplitude of the globally-averaged annual CO₂ cycle is also affected by the atmosphere-ocean
770 CO₂ fluxes makes it more difficult to attribute the changes in the amplitude of the globally-
771 averaged annual CO₂ cycle solely to atmosphere-land CO₂ fluxes. Additionally, the increase in
772 crop area as well as crop yield per unit area over the historical period have been suggested by
773 Zeng et al. (2014) to contribute towards the observed increase in the amplitude of annual CO₂
774 cycle. Based on their sensitivity tests, Zeng et al. (2014) attribute 45, 29 and 26 percent of the
775 observed increase in the seasonal-cycle amplitude of the CO₂ cycle to LUC, climate variability
776 and change (including factors such as the lengthening of the growing season) and increased
777 productivity due to CO₂ fertilization, respectively. Comparison of the rate of increase of NPP in
778 CanESM4.2 experiments with and without LUC (Figure 10b), as a measure of increase in the
779 strength of the CO₂ fertilization effect, suggests that the contribution of anthropogenic LUC to the
780 increase in the seasonal-cycle amplitude is 52%, which is broadly consistent with the 45% value
781 obtained by Zeng et al. (2014).

782
783 While CanESM4.2 simulation with $\gamma_d=0.40$ is able to simulate a realistic rate of increase of
784 $[\text{CO}_2]$ over the period 1960 to 2005, the modelled atmosphere-ocean CO_2 fluxes for this and the
785 CanESM2 version are lower than observational estimates of this quantity (Figure 8). This implies
786 that if the modelled atmosphere-ocean CO_2 flux were to increase and become more consistent
787 with observation-based estimates then the modelled atmosphere-land CO_2 flux must decrease to
788 still be able to yield sufficiently realistic rate of increase of $[\text{CO}_2]$. This implies that the strength
789 of the terrestrial CO_2 fertilization effect should likely be somewhat lower than what is obtained by
790 $\gamma_d=0.40$ or the simulated atmosphere-land CO_2 flux is higher because of some other reason, most
791 likely lower LUC emissions. Indeed, the required decrease in modelled atmosphere-land CO_2 flux
792 is consistent with the fact that the modelled LUC emissions for $\gamma_d=0.40$ (81 Pg C) are about half
793 the estimate from Houghton (2008) (156 Pg C) with the caveat, of course, that Houghton's
794 estimates themselves have an uncertainty of roughly $\pm 50\%$. The LUC module of CTEM currently
795 only accounts for changes in crop area and does not take into account changes associated with
796 pasture area given their ambiguous definition (pasture may or may not be grasslands). The model
797 also does not take into account wood harvesting which amongst other uses is also used as a
798 biofuel. Treatment of these additional processes will increase modelled LUC emissions.

799
800 Although the CanESM4.2 simulation with $\gamma_d=0.40$ satisfies three out of four constraints placed
801 by the chosen determinants of the global carbon cycle and the historical carbon budget, and also
802 simulates reasonable soil carbon loss in response to anthropogenic LUC, the model now yields
803 the highest land carbon uptake, in the 1pctCO2 experiment, amongst the CMIP5 models that were
804 compared by Arora et al. (2013) as seen in Figure 2. Of course, the 1pctCO2 experiment is in no

805 way indicative of models' performance over the historical period, nor is being an outlier amongst
806 CMIP5 models a conclusive evaluation of CanESM4.2's land carbon uptake. However, it remains
807 possible that the chosen determinants of the global carbon cycle and the historical carbon budget
808 are not able to constrain the model sufficiently, given the especially large uncertainty associated
809 with LUC emissions. Nevertheless, these observation-based constraints of the carbon cycle and
810 historical carbon budget are essentially the only means to evaluate carbon cycle aspects of the
811 ESMs at the global scale including the strength of the terrestrial CO₂ fertilization effect. In the
812 near future, availability of model output from the sixth phase of CMIP (CMIP6) will allow a
813 comparison of the simulated aspects of the global carbon cycle and the historical carbon budget
814 from ESMs to observations-based estimates for the 1850-2014 period. These data will allow a
815 comparison of the rate of increase of the amplitude of globally-averaged surface [CO₂] in models
816 with observation-based estimates over a longer period. This should help better constrain the
817 strength of the terrestrial CO₂ fertilization effect, as it is represented in models, in a somewhat
818 more robust manner.

819

820 **6.0 Source code and data availability**

821 Source code for the complete CanESM4.2 model is an extremely complex set of FORTRAN
822 subroutines, with C preprocessor (CPP) directives, that reside in CCCma libraries. Unix shell
823 scripts process the model code for compilation based on CPP directives and several other
824 switches (e.g. those related to free-CO₂, specified-CO₂, and relaxed-CO₂ settings). As such, it is
825 extremely difficult to make the full model code available. However, selected model subroutines
826 related to specific physical and biogeochemical processes can be made available by either author
827 (vivek.arora@canada.ca, john.scinocca@canada.ca) upon agreeing to Environment and Climate

828 Change Canada's software licensing agreement available at
829 <http://collaboration.cmc.ec.gc.ca/science/rpn.comm/license.html>. Data used to produce plots and
830 figures can be obtained from the first author (vivek.arora@canada.ca).

831

832 **Copyright statement**

833 The works published in this journal are distributed under the Creative Commons Attribution 3.0
834 License. This license does not affect this Crown copyright work, which is re-usable under the
835 Open Government License (OGL). The Creative Commons Attribution 3.0 License and the OGL
836 are interoperable and do not conflict with, reduce or limit each other. ©Crown copyright 2015.

837

838 **Acknowledgements**

839 We would like to thank Joe Melton and Neil Swart for providing comments on an earlier version
840 of this paper. We also thank the three anonymous reviewers for their constructive and helpful
841 comments.

842

843 **References**

- 844 Arora, V. K. and Boer, G. J. (2005) A parameterization of leaf phenology for the terrestrial ecosystem
845 component of climate models, *Glob. Change Biol.*, 11, 39–59, doi:10.1111/j.1365-
846 2486.2004.00890.x.
- 847 Arora, V. K. and Boer, G. J. (2014) Terrestrial ecosystems response to future changes in climate and
848 atmospheric CO₂ concentration, *Biogeosciences*, 11, 4157-4171, doi:10.5194/bg-11-
849 4157-2014Arora, V. K. and Boer, G. J. (2014) Terrestrial ecosystems response to future
850 changes in climate and atmospheric CO₂ concentration, *Biogeosciences Discuss.*, 11,
851 3581-3614, doi:10.5194/bgd-11-3581-2014.
- 852 Arora, V. K., G. J. Boer, J. R. Christian, C. L. Curry, K. L. Denman, K. Zahariev, G. M. Flato, J. F.
853 Scinocca, W. J. Merryfield, and W. G. Lee (2009) The effect of terrestrial photosynthesis
854 down-regulation on the 20th century carbon budget simulated with the CCCma Earth
855 System Model, *J. Clim.*, 22, 6066-6088.
- 856 Arora, V. K., G. J. Boer, P. Friedlingstein, M. Eby, C. D. Jones, J. R. Christian, G. Bonan, L. Bopp,
857 V. Brovkin, P. Cadule, T. Hajima, T. Ilyina, K. Lindsay, J. F. Tjiputra, T. Wu (2013)
858 Carbon-Concentration and Carbon-Climate Feedbacks in CMIP5 Earth System Models.
859 *Journal of Climate*, Vol. 26, Iss. 15, pp. 5289-5314.
- 860 Arora, V. K., J. F. Scinocca, G. J. Boer, J. R. Christian, K. L. Denman, G. M. Flato, V. V. Kharin, W.
861 G. Lee, and W. J. Merryfield (2011) Carbon emission limits required to satisfy future
862 representative concentration pathways of greenhouse gases, *Geophys. Res. Lett.*, 38,
863 L05805, doi:10.1029/2010GL046270.
- 864 Arora, V.K. and G.J. Boer (2010) Uncertainties in the 20th century carbon budget associated with
865 land use change, *Global Change Biology*, 16(12), 3327-3348.
- 866 Bartlett, P. A., Mackay, M. D., and Verseghy, D. L. (2006) Modified snow algorithms in the Canadian
867 Land Surface Scheme: model runs and sensitivity analysis at three boreal forest stands,
868 *Atmos. Ocean*, 44, 207–222.
- 869 Bartlett, P. and Verseghy, D. (2015) Modified treatment of intercepted snow improves the
870 simulated forest albedo in the Canadian Land Surface Scheme, *Hydrol. Process.*, 29, 3208–
871 3226, doi:10.1002/hyp.10431.
- 872 Brown, R., Bartlett, P., Mackay, M., and Verseghy, D. (2006) Estimation of snow cover in CLASS for
873 SnowMIP, *Atmos. Ocean*, 44, 223–238.

874 Christian, J. R., and coauthors (2010) The global carbon cycle in the Canadian Earth system model
875 (CanESM1): Preindustrial control simulation, *J. Geophys. Res.*, 115, G03014,
876 doi:10.1029/2008JG000920.

877 Ciais, P., C. Sabine, G. Bala, L. Bopp, V. Brovkin, J. Canadell, A. Chhabra, R. DeFries, J. Galloway,
878 M. Heimann, C. Jones, C. Le Quéré, R.B. Myneni, S. Piao and P. Thornton (2013) Carbon
879 and Other Biogeochemical Cycles. In: *Climate Change 2013: The Physical Science Basis.*
880 *Contribution of Working Group I to the Fifth Assessment Report of the Intergovernmental*
881 *Panel on Climate Change [Stocker, T.F., D. Qin, G.-K. Plattner, M. Tignor, S.K. Allen, J.*
882 *Boschung, A. Nauels, Y. Xia, V. Bex and P.M. Midgley (eds.)]. Cambridge University*
883 *Press, Cambridge, United Kingdom and New York, NY, USA.*

884 da Rocha, H.R., M.L. Goulden, S.D. Miller, M.C. Menton, L.D.V.O. Pinto, H.C. De Freitas, and
885 A.M.E. Silva Figueira (2004): Seasonality of water and heat fluxes over a tropical forest
886 in eastern Amazonia, *Ecological Applications*, 14(4) Supplement, S22-S32.

887 Friedlingstein, P., P. Cox, R. Betts, L. Bopp, W. von Bloh, V. Brovkin, P. Cadule, S. Doney, M. Eby,
888 I. Fung, G. Bala, J. John, C. Jones, F. Joos, T. Kato, M. Kawamiya, W. Knorr, K. Lindsay,
889 H. D. Matthews, T. Raddatz, P. Rayner, C. Reick, E. Roeckner, K.-G. Schnitzler, R.
890 Schnur, K. Strassmann, A. J. Weaver, C. Yoshikawa, N. Zeng. 2006: Climate–carbon
891 cycle feedback analysis: Results from the C4MIP model intercomparison, *J. Clim.*, 19(14),
892 3337-3353.

893 G. C. Hurtt, L. P. Chini, S. Frolking, R. A. Betts, J. Feddema, G. Fischer, J. P. Fisk, K. Hibbard, R. A.
894 Houghton, A. Janetos, C. D. Jones, G. Kindermann, T. Kinoshita, Kees Klein Goldewijk,
895 K. Riahi, E. Shevliakova, S. Smith, E. Stehfest, A. Thomson, P. Thornton, D. P. van
896 Vuuren, Y. P. Wang (2011) Harmonization of land-use scenarios for the period 1500-
897 2100: 600 years of global gridded annual land-use transitions, wood harvest, and resulting
898 secondary lands. *Climatic Change*, 109, 117-161, doi:10.1007/s10584-011-0153-2.

899 Garnaud, C., L. Sushama, V. K. Arora (2014) The effect of driving climate data on the simulated
900 terrestrial carbon pools and fluxes over North America, *International Journal of*
901 *Climatology* 34 (4), 1098-1110.

902 Gillett, N. P., V. K. Arora, D. Matthews, M. R. Allen (2013) Constraining the Ratio of Global
903 Warming to Cumulative CO₂ Emissions Using CMIP5 Simulations. *Journal of Climate*,
904 Vol. 26, Iss. 18, pp. 6844-6858.

905 Gourdji, S. M., K. L. Mueller, V. Yadav, D. N. Huntzinger, A. E. Andrews, M. Trudeau, G. Petron, T.
906 Nehrkorn, J. Eluszkiewicz, J. Henderson, D. Wen, J. Lin, M. Fischer, C. Sweeney, and A.
907 M. Michalak (2012) North American CO₂ exchange: inter-comparison of modeled
908 estimates with results from a fine-scale atmospheric inversion, *Biogeosciences*, 9, 457–
909 475, doi:10.5194/bg-9-457-2012.

910 Hoffman, F. M., J. T. Randerson, V. K. Arora, Q. Bao, P. Cadule, D. Ji, C. D. Jones, M. Kawamiya,
911 S. Khatiwala, K. Lindsay, A. Obata, E. Shevliakova, K. D. Six, J. F. Tjiputra, E. M.
912 Volodin, and T. Wu (2014) Causes and implications of persistent atmospheric
913 carbondioxide biases in Earth System Models, *J. Geophys. Res. Biogeosci.*, 119, 141–162,
914 doi:10.1002/2013JG002381.

915 Houghton, R.A. 2008. Carbon Flux to the Atmosphere from Land-Use Changes: 1850-2005. In
916 *TRENDS: A Compendium of Data on Global Change. Carbon Dioxide Information*
917 *Analysis Center, Oak Ridge National Laboratory, U.S. Department of Energy, Oak Ridge,*
918 *Tenn., U.S.A.*

919 Jones, C., E. Robertson, V. Arora, P. Friedlingstein, E. Shevliakova, L. Bopp, V. Brovkin, T. Hajima,
920 E. Kato, M. Kawamiya, S. Liddicoat, K. Lindsay, C.H. Reick, C. Roelandt, J.
921 Segschneider, J. Tjiputra (2013) Twenty-First-Century Compatible CO₂ Emissions and
922 Airborne Fraction Simulated by CMIP5 Earth System Models under Four Representative
923 Concentration Pathways. *Journal of Climate*, Vol. 26, Iss. 13, pp. 4398-4413.

924 Keeling, C. D., Chin, J. F. S. & Whorf, T. P. (1996) Increased activity of northern vegetation inferred
925 from atmospheric CO₂ measurements. *Nature* 382, 146–149.

926 Khatiwala, S., F. Primeau, and T. Hall (2009) Reconstruction of the history of anthropogenic CO₂
927 concentrations in the ocean. *Nature*, 462, 346–349.

928 Knol, M. J., W. R. Pestman, and D. E. Grobbee (2011) The (mis)use of overlap of confidence
929 intervals to assess effect modification, *Eur. J. Epidemiol.*, 26(4), 253–254.

930 Knorr, W. (2009) Is the airborne fraction of anthropogenic CO₂ emissions increasing?, *Geophys. Res.*
931 *Lett.*, 36, L21710, doi:10.1029/2009GL040613.

932 Le Quéré, C., Moriarty, R., Andrew, R. M., Peters, G. P., Ciais, P., Friedlingstein, P., Jones, S. D.,
933 Sitch, S., Tans, P., Armeth, A., Boden, T. A., Bopp, L., Bozec, Y., Canadell, J. G., Chini,
934 L. P., Chevallier, F., Cosca, C. E., Harris, I., Hoppema, M., Houghton, R. A., House, J. I.,
935 Jain, A. K., Johannessen, T., Kato, E., Keeling, R. F., Kitidis, V., Klein Goldewijk, K.,
936 Koven, C., Landa, C. S., Landschützer, P., Lenton, A., Lima, I. D., Marland, G., Mathis, J.

937 T., Metzl, N., Nojiri, Y., Olsen, A., Ono, T., Peng, S., Peters, W., Pfeil, B., Poulter, B.,
938 Raupach, M. R., Regnier, P., Rödenbeck, C., Saito, S., Salisbury, J. E., Schuster, U.,
939 Schwinger, J., Séférian, R., Segschneider, J., Steinhoff, T., Stocker, B. D., Sutton, A. J.,
940 Takahashi, T., Tilbrook, B., van der Werf, G. R., Viovy, N., Wang, Y.-P., Wanninkhof,
941 R., Wiltshire, A., and Zeng, N. (2015) Global carbon budget 2014, *Earth Syst. Sci. Data*,
942 7, 47-85, doi:10.5194/essd-7-47-2015.

943 Ma, X., von Salzen, K., and Li, J. (2008) Modelling sea salt aerosol and its direct and indirect effects
944 on climate, *Atmos. Chem. Phys.*, 8, 1311–1327, doi:10.5194/acp-8-1311-2008.

945 McGuire, A. D., J. M. Melilli, and L. A. Joyce (1995): The role of nitrogen in the response of forest
946 net primary productivity to elevated atmospheric carbon dioxide, *Annual Reviews of*
947 *Ecology and Systematics*, 26, 473-503.

948 Medlyn, B. E., F. -W. Badeck, D. G. G. De Pury, C. V. M. Barton, M. Broadmeadow, R. Ceulemans,
949 P. De Angelis, M. Forstreuter, M. E. Jach, S. Kellomäki, E. Laitat, M. Marek, S. Philippot,
950 A. Rey, J. Strassmeyer, K. Laitinen, R. Liozon, B. Portier, P. Roberntz, K. Wang, P. G.
951 Jstbid (1999): Effects of elevated [CO₂] on photosynthesis in European forest species: a
952 meta-analysis of model parameters, *Plant, Cell & Environment*, 22, 1475–1495.

953 Melton, J. R. and Arora, V. K. (2014) Sub-grid scale representation of vegetation in global land
954 surface schemes: implications for estimation of the terrestrial carbon sink, *Biogeosciences*,
955 11, 1021-1036, doi:10.5194/bg-11-1021-2014.

956 Melton, J. R. and Arora, V. K. (2014) Sub-grid scale representation of vegetation in global land
957 surface schemes: implications for estimation of the terrestrial carbon sink, *Biogeosciences*,
958 11, 1021-1036, doi:10.5194/bg-11-1021-2014.

959 Melton, J. R., Shrestha, R. K., and Arora, V. K. (2015) The influence of soils on heterotrophic
960 respiration exerts a strong control on net ecosystem productivity in seasonally dry
961 Amazonian forests, *Biogeosciences*, 12, 1151-1168, doi:10.5194/bg-12-1151-2015.

962 Namazi, M., von Salzen, K., and Cole, J. N. S. (2015) Simulation of black carbon in snow and its
963 climate impact in the Canadian Global Climate Model, *Atmos. Chem. Phys. Discuss.*, 15,
964 18839-18882, doi:10.5194/acpd-15-18839-2015.

965 Peng, Y., Arora, V. K., Kurz, W. A., Hember, R. A., Hawkins, B. J., Fyfe, J. C., and Werner, A. T.
966 (2014) Climate and atmospheric drivers of historical terrestrial carbon uptake in the
967 province of British Columbia, Canada, *Biogeosciences*, 11, 635-649, doi:10.5194/bg-11-
968 635-2014.

969 Peng, Y., von Salzen, K., and Li, J. (2012) Simulation of mineral dust aerosol with Piecewise Log-
970 normal Approximation (PLA) in CanAM4-PAM, *Atmos. Chem. Phys.*, 12, 6891–6914, 30
971 doi:10.5194/acp-12-6891-2012.

972 Phillips, O. L. and S. L. Lewis (2014) Evaluating the tropical forest carbon sink, *Global Change*
973 *Biology* (2014) 20, 2039–2041, doi: 10.1111/gcb.12423.

974 Pongratz, J., Reick, C. H., Houghton, R. A., and House, J. I. (2014) Terminology as a key uncertainty
975 in net land use and land cover change carbon flux estimates, *Earth Syst. Dynam.*, 5, 177-
976 195, doi:10.5194/esd-5-177-2014.

977 Ramankutty, N., H. K. Gibbs, F. Archard, R. DeFries, J. A. Foley, and R. A. Houghton (2007):
978 Challenges to estimating carbon emissions from tropical deforestation , *Global Change*
979 *Biology*, 13(1), 51-66.

980 Randerson, J. T., Thompson, M. V., Conway, T. J., Fung, I. Y. & Field, C. B. (1997) The contribution
981 of terrestrial sources and sinks to trends in the seasonal cycle of atmospheric carbon
982 dioxide. *Glob. Biogeochem. Cycles* 11, 535–560.

983 Schimel, D., Stephens, B. B., and Fisher, J. B.: Effect of increasing CO₂ on the terrestrial carbon
984 cycle (2015) *Proceedings of the National Academy of Science U.S.A.*, 112, 436–441,
985 doi:10.1073/pnas.1407302112, 2015.

986 Sturm, M., Holmgren, J., König, M., and Morris, K. (1997) The thermal conductivity of seasonal
987 snow, *J. Glaciol.*, 43, 26–41.

988 Tabler, R. D., Benson, C. S., Santana, B. W., and Ganguly, P. (1990) Estimating snow transport from
989 30 wind speed records: estimates versus measurements at Prudhoe Bay, Alaska, in: *Proc.*
990 *58th Western Snow Conf.*, Sacramento, CA, 61–78.

991 Taylor, Karl E., Ronald J. Stouffer, Gerald A. Meehl, 2012: An Overview of CMIP5 and the
992 Experiment Design. *Bull. Amer. Meteor. Soc.*, 93, 485–498.

993 Verseghy, D. L. (2012) CLASS-the Canadian land surface scheme (version 3.6)—technical
994 documentation. Internal report, Climate Research Division, Science and Technology
995 Branch, Environment Canada (Downsview, Toronto, Ontario)

996 von Salzen, K. (2006) Piecewise log-normal approximation of size distributions for aerosol
997 modelling, *Atmos. Chem. Phys.*, 6, 1351–1372, doi:10.5194/acp-6-1351-2006.

998 von Salzen, K., and Coauthors, 2013: The Canadian fourth generation atmospheric global climate
999 model (CanAM4). Part I: Representation of physical processes. *Atmos. Ocean*, 51,
1000 doi:10.1080/07055900.2012.75561.

1001 Wei, X., M. Shao, W. Gale and L. Li (2014) Global pattern of soil carbon losses due to the conversion
1002 of forests to agricultural land, *Scientific Reports* 4, Article number: 4062 (2014)
1003 doi:10.1038/srep04062.

1004 Zaehle, S., Medlyn, B. E., De Kauwe, M. G., Walker, A. P., Dietze, M. C., Hickler, T., Luo, Y.,
1005 Wang, Y.-P., El-Masri, B., Thornton, P., Jain, A., Wang, S., Warlind, D., Weng, E.,
1006 Parton, W., Iversen, C. M., Gallet-Budynek, A., McCarthy, H., Finzi, A., Hanson, P. J.,
1007 Prentice, I. C., Oren, R., and Norby, R. (2014) Evaluation of 11 terrestrial carbon–nitrogen
1008 cycle models against observations from two temperate Free-Air CO₂ Enrichment studies,
1009 *New Phytologist*, 202, 803–822, doi:10.1111/nph.12697.

1010 Zeng, N., Zhao, F., Collatz, G. J., Kalnay, E., Salawitch, R. J., West, T. O., Guanter, L. (2014) .
1011 Agricultural Green Revolution as a driver of increasing atmospheric CO₂ seasonal
1012 amplitude, *Nature*, 515(7527), 394-397.

1013 Zobler, L. 1986. A World Soil File for Global Climate Modelling. NASA Technical Memorandum
1014 87802. NASA Goddard Institute for Space Studies, New York, New York, U.S.A.

1015

1016

1017 Table 1: Summary of simulations performed for this study and the forcings used.

Simulation	1pctCO2	esmhistorical	esmhistorical_noluc
Simulation details	1% per year increasing CO ₂ simulation	1850-2005 historical simulation based on CMIP5 protocol	1850-2005 historical simulation based on CMIP5 protocol, but with no anthropogenic land use change
Purpose	To allow comparison of CanESM4.2 with CMIP5 models especially in terms of its land carbon uptake	To compare simulated aspects of the global carbon cycle and historical carbon budget with observation-based estimates	To diagnose LUC emissions by differencing atmosphere-land CO ₂ flux between historical simulations with and without LUC.
Length	140 years	156 years	
CO ₂ forcing	285 ppm at the start of the simulation and 1140 ppm after 140 years.	Historical CO ₂ forcing	
Land cover forcing	Land cover corresponds to its 1850 state	Land cover evolution is based on increase in crop area over the historical period	Land cover corresponds to its 1850 state
Non-CO ₂ greenhouse gases forcing	Concentration of non-CO ₂ GHGs is specified at their 1850 levels.	Concentration of non-CO ₂ GHGs is specified and evolves over the historical period based on the CMIP5 protocol	
Aerosols forcing	Emissions of aerosols and their precursors are specified at their 1850 levels.	Emissions of aerosols and their precursors are specified and evolve over the historical period based on the CMIP5 protocol	

1018

1019

1020

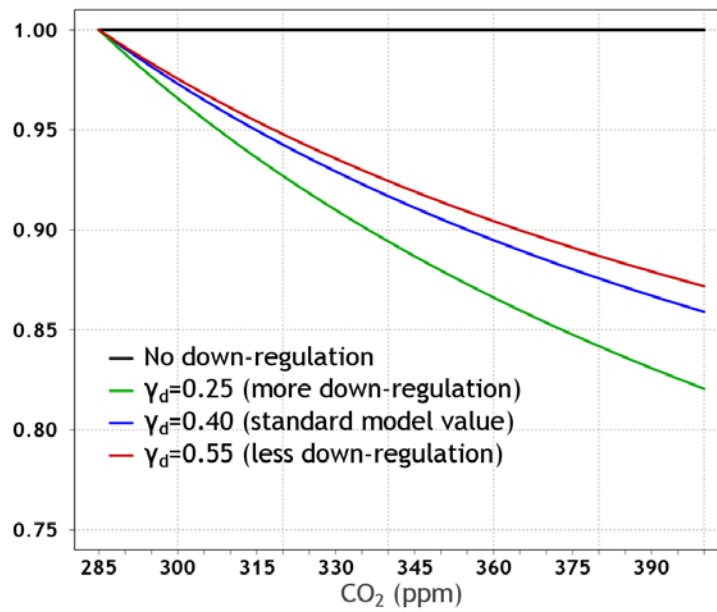
1021

1022

1023

1024

Down-regulation factor as a function of CO₂ concentration



1025

1026 Figure 1: The behaviour of terrestrial photosynthesis down-regulation scalar $\xi(C)$ (equation 12)

1027 for $\gamma_p=0.95$ and values of γ_d equal to 0.25, 0.4 and 0.55 that are used in CanESM4.2 simulations.

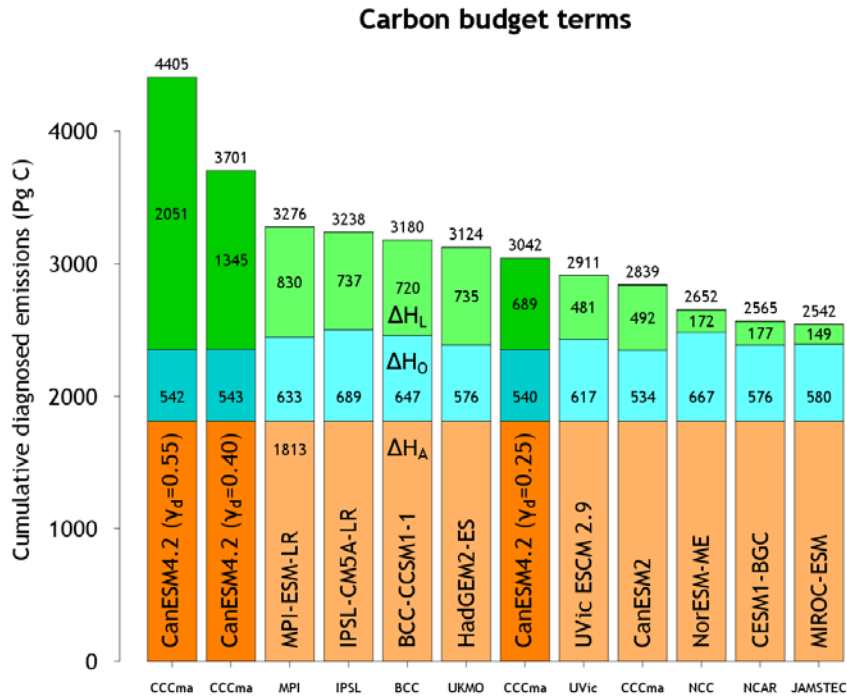
1028

1029

1030

1031

1032



1033

1034

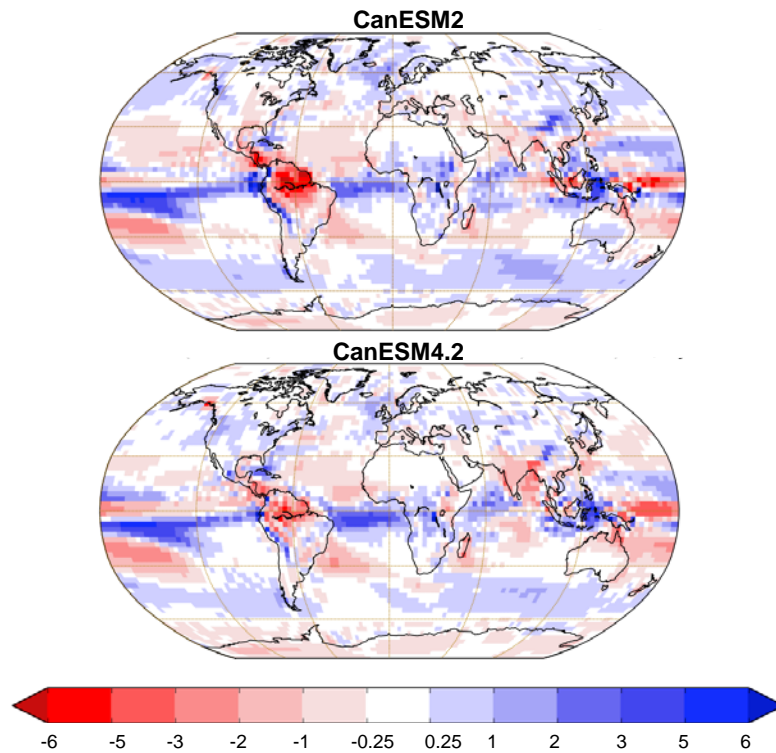
1035 Figure 2: Components of the carbon budget equation (8) that make up cumulative diagnosed
 1036 emissions based on results from the fully-coupled 1pctCO2 experiment. Results shown are from
 1037 eight CMIP5 models that participated in the Arora et al. (2013) study and from three CanESM4.2
 1038 simulations (shown in darker colours) for three different strengths of the terrestrial CO₂
 1039 fertilization effect.

1040

1041

1042

Model minus Xie and Arkin precipitation
averaged over the 1979-1998 period (mm/day)



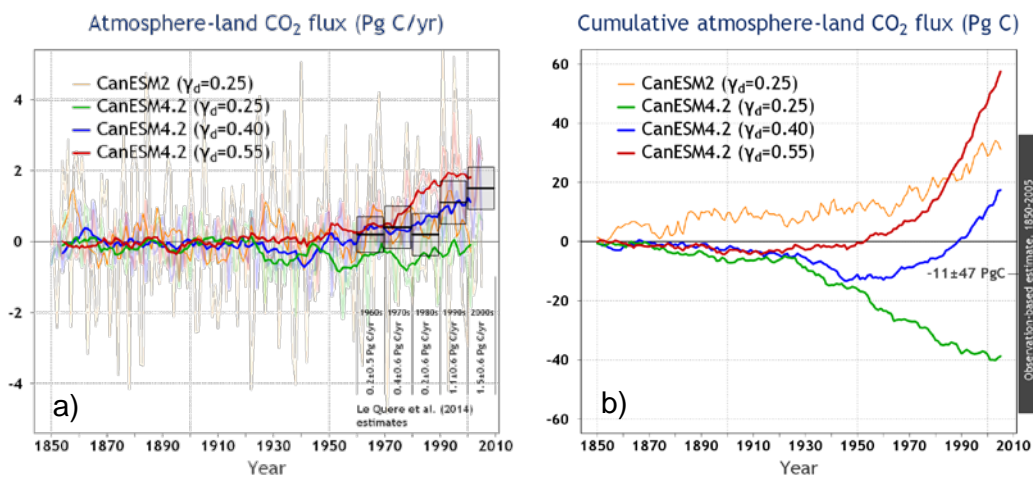
1043

1044

1045 Figure 3: CanESM2 (panel a) and CanESM4.2 (panel b, $\gamma_d=0.40$) precipitation anomalies
1046 compared to the observation-based estimates from CPC Merged Analysis of Precipitation
1047 (CMAP) based on Xie and Arkin (1997) averaged over the 1979–1998 period.

1048

1049
1050
1051
1052
1053

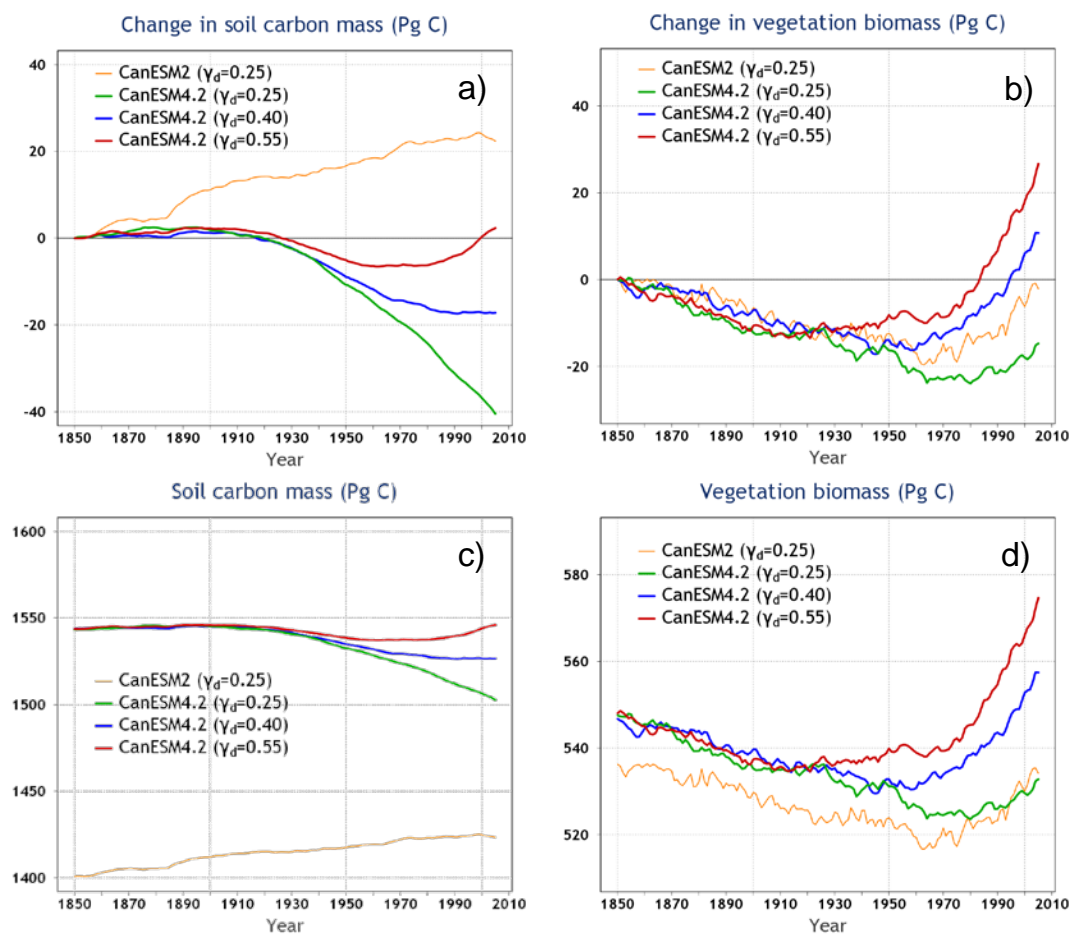


1054

1055 Figure 4: Atmosphere-land CO₂ flux (F_L) (panel a) and its cumulative values \tilde{F}_L (panel b) from
1056 CanESM2 and the three CanESM4.2 historical 1850-2005 simulations for different strengths of
1057 the terrestrial CO₂ fertilization effect. In panel (a) the observation-based estimates of F_L and their
1058 uncertainty, show via boxes, for the decades of 1960, 1970, 1980, 1990 and 2000 are reproduced
1059 from Le Quéré et al. (2015). The bold lines in panel (a) are the 10-year moving averages of the
1060 annual F_L values which are shown in light colours. The results from CanESM2 and CanESM4.2
1061 are the average of the two ensemble members.

1062

1063



1065

1066 Figure 5: Change in and absolute values of global soil carbon and vegetation biomass amounts
 1067 from CanESM2 and the three CanESM4.2 historical 1850-2005 simulations with different
 1068 strengths of the terrestrial CO₂ fertilization effect. The results shown in all panels are the average
 1069 of the two ensemble members.

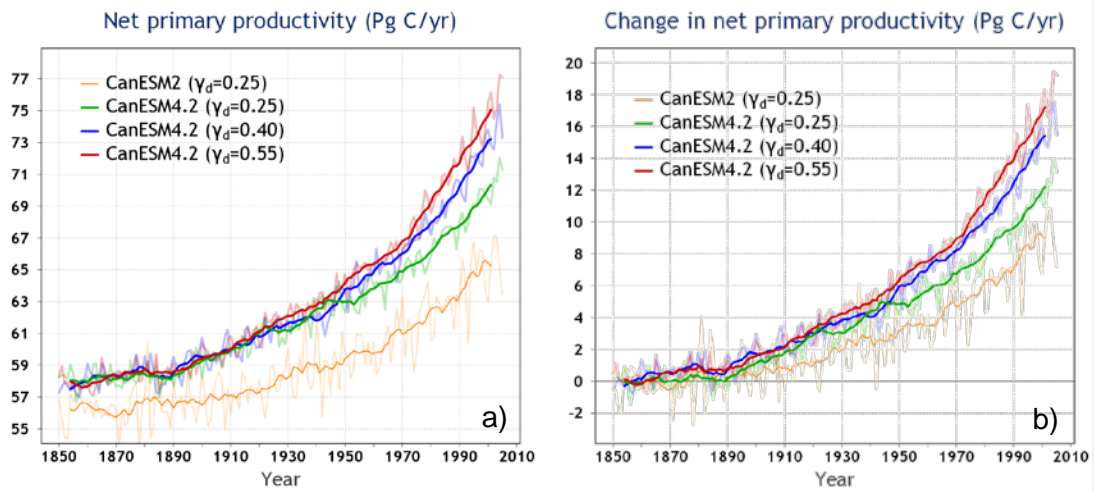
1070

1071

1072

1073

1074



1075

1076 Figure 6: Absolute values of (panel a), and change in (panel b), net primary productivity (NPP)
1077 from CanESM2 and the three CanESM4.2 historical 1850-2005 simulations with different
1078 strengths of the terrestrial CO₂ fertilization effect. The thin lines show the ensemble-mean based
1079 on results from the two ensemble members and the bold lines are their 10-year moving averages.

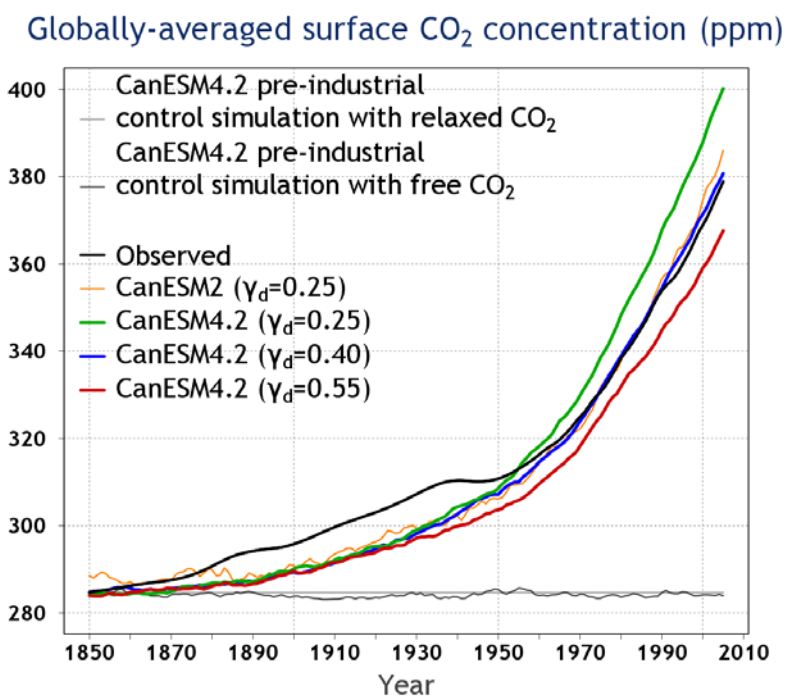
1080

1081

1082

1083

1084

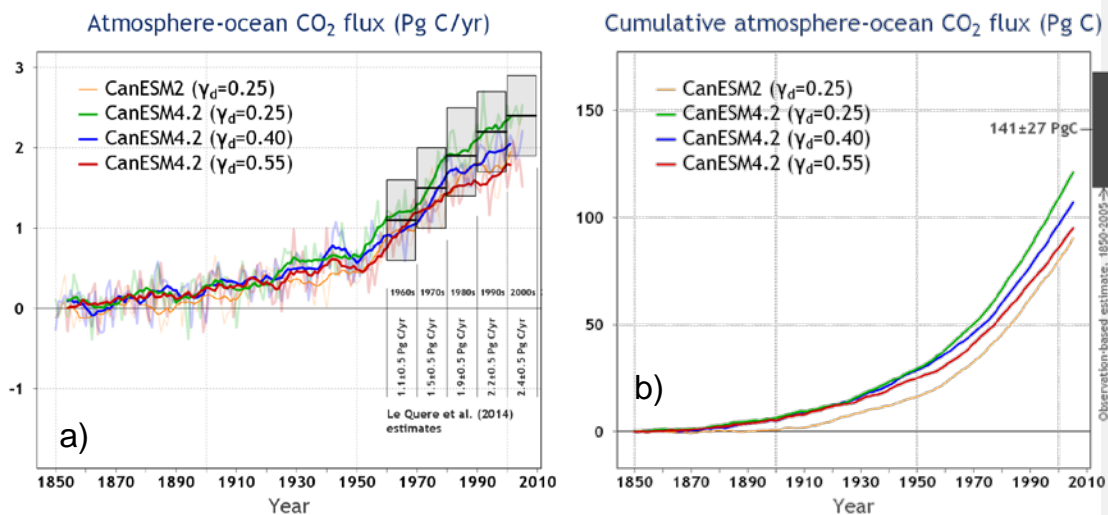


1085

1086 Figure 7: Simulated globally-averaged surface atmospheric CO₂ concentration from CanESM2
1087 and the three CanESM4.2 historical 1850-2005 simulations with different strengths of the
1088 terrestrial CO₂ fertilization effect. The observation-based concentration is shown in black. Also
1089 shown is the CO₂ concentration of 284.6 ppm used in CanESM4.2's pre-industrial simulation in
1090 the relaxed-CO₂ configuration and the simulated concentration from the pre-industrial
1091 CanESM4.2 simulation with interactively determined CO₂.

1092

1093
1094
1095

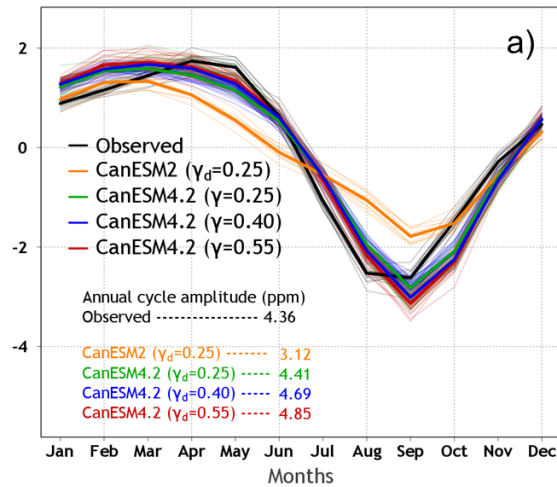


1096

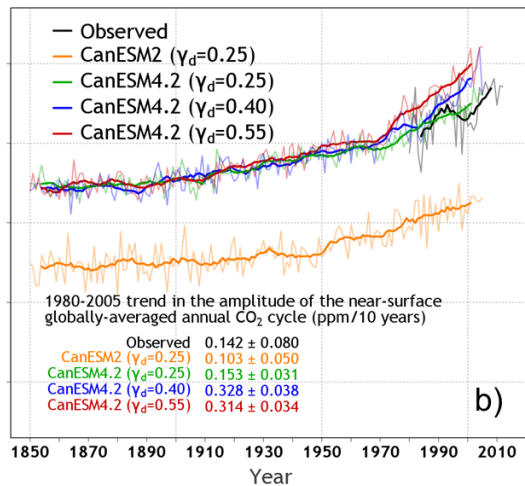
1097 Figure 8: Atmosphere-ocean CO₂ flux (F_O) (panel a) and its cumulative values \tilde{F}_O (panel b) from
1098 CanESM2 and the three CanESM4.2 historical 1850-2005 simulations for three different
1099 strengths of the terrestrial CO₂ fertilization effect. In panel (a) the observation-based estimates of
1100 F_O and their uncertainty, show via boxes, for the decades of 1960, 1970, 1980, 1990 and 2000 are
1101 reproduced from Le Quéré et al. (2015). The bold lines in panel (a) are the 10-year moving
1102 averages of the annual F_L values which are shown in light colours. The results from CanESM2
1103 and CanESM4.2 are the average of the two ensemble members.

1104
1105

Monthly CO₂ cycle trend-adjusted anomalies (ppm) 1991-2000



Amplitude of the globally-averaged annual CO₂ cycle (ppm)



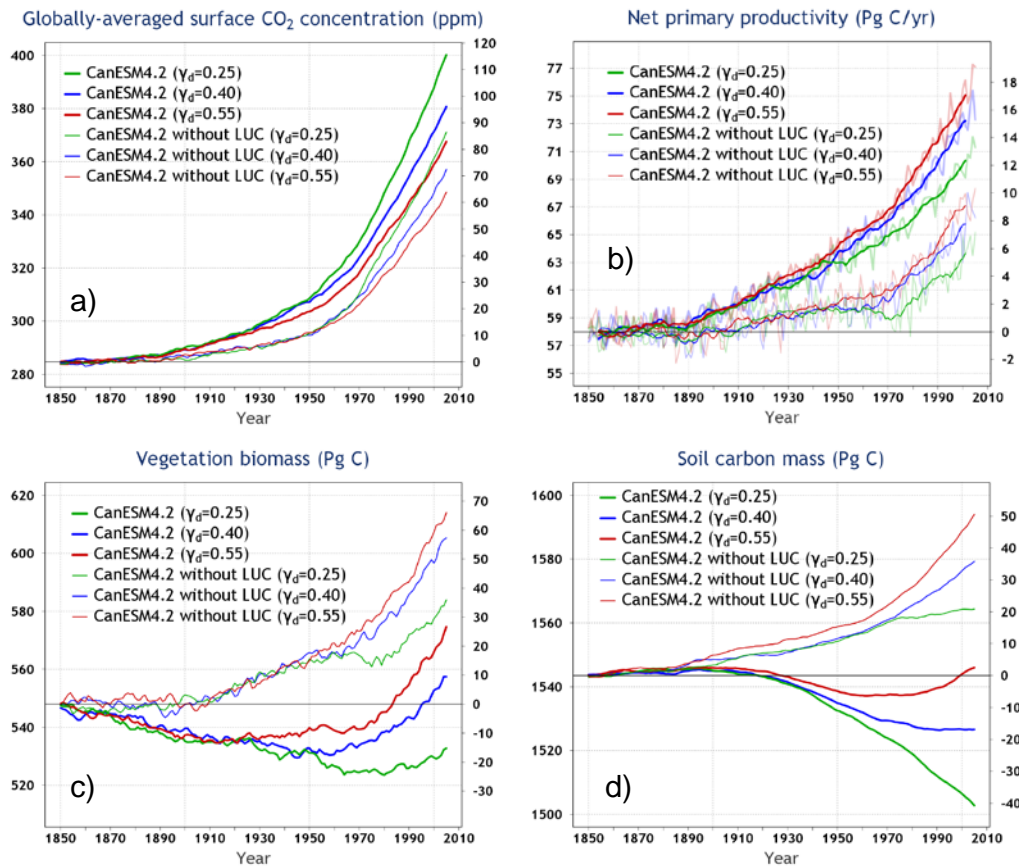
1106

1107 Figure 9: The annual cycle of trend-adjusted globally-averaged near-surface monthly [CO₂]
 1108 anomalies from CanESM2, the versions of CanESM4.2 for three different strengths of the CO₂
 1109 fertilization effect and observation-based estimates for the 1991-2000 period (panel a). Panel (b)
 1110 shows the time series of the amplitude of the annual cycle of the trend adjusted globally-averaged
 1111 near-surface monthly [CO₂] anomalies for corresponding model and observation-based estimates.
 1112 The bold lines are 10-year moving averages and the thin lines for model results are the average of
 1113 results from two ensemble members.

1114

1115

1116



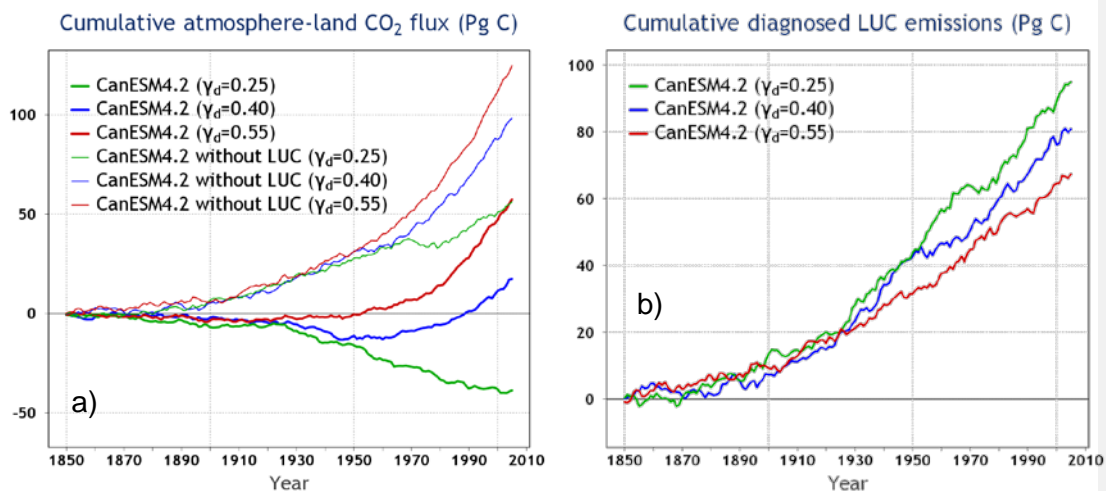
1117

1118 Figure 10: Comparison of CanESM4.2 simulations with and without implementation of
1119 anthropogenic land use change over the historical period for three different strengths of the
1120 terrestrial CO₂ fertilization effect: a) Globally-averaged annual surface atmospheric CO₂
1121 concentration, b) net primary productivity, c) global vegetation biomass, and c) global soil carbon
1122 mass. All lines are the average of results from two ensemble members. Additionally, in panel (b)
1123 the bold lines are the 10-year moving averages.

1124

1125

1126
1127



1128
1129
1130
1131
1132
1133
1134
1135
1136
1137
1138

Figure 11: Comparison of simulated cumulative atmosphere-land CO₂ flux from CanESM4.2 simulations with and without implementation of anthropogenic land use change over the historical period for three different strengths of the terrestrial CO₂ fertilization (panel a). Panel (b) shows the cumulative diagnosed LUC emissions calculated using equation (10) as the difference between cumulative atmosphere-land CO₂ flux from simulations with and without LUC shown in panel (a). All lines are the average of results from two ensemble members.